

## **General Disclaimer**

### **One or more of the Following Statements may affect this Document**

- This document has been reproduced from the best copy furnished by the organizational source. It is being released in the interest of making available as much information as possible.
- This document may contain data, which exceeds the sheet parameters. It was furnished in this condition by the organizational source and is the best copy available.
- This document may contain tone-on-tone or color graphs, charts and/or pictures, which have been reproduced in black and white.
- This document is paginated as submitted by the original source.
- Portions of this document are not fully legible due to the historical nature of some of the material. However, it is the best reproduction available from the original submission.



FEASIBILITY STUDY OF VACUUM GAUGING  
USING ELECTRON-INDUCED SOFT X-RAYS

By  
Kirtland H. Olson  
Joseph L. Wiza  
Andrew J. Borsa  
July 1969

Distribution of this report is provided in the interest of information exchange and should not be construed as endorsement by NASA of the material presented. Responsibility for the contents resides in the organization that prepared it.

Prepared under Contract No. NAS 12-2127 by

LOWELL TECHNOLOGICAL INSTITUTE RESEARCH FOUNDATION  
Lowell, Massachusetts

Electronics Research Center  
NATIONAL AERONAUTICS AND SPACE ADMINISTRATION

FACILITY FORM 802

N70-10330

(ACCESSION NUMBER) 83

(PAGES) 24

(THRU) 1

(CODE) 24

(CATEGORY)

(NASA CR OR TMX OR AD NUMBER)

FEASIBILITY STUDY OF VACUUM GAUGING  
USING ELECTRON-INDUCED SOFT X-RAYS

By

Kirtland H. Olson

Joseph L. Wiza

Andrew J. Borsa

July 1969

Prepared under Contract No. NAS 12-2127 by  
LOWELL TECHNOLOGICAL INSTITUTE RESEARCH FOUNDATION  
Lowell, Massachusetts

Electronics Research Center  
NATIONAL AERONAUTICS AND SPACE ADMINISTRATION

## TABLE OF CONTENTS

	Page
1.0 INTRODUCTION	1
2.0 EXPERIMENTAL ARRANGEMENT	5
2.1 Vacuum System	5
2.2 Electronics Rack	8
2.3 Detection	12
3.0 SYSTEM ANALYSIS	17
3.1 The Bremsstrahlung Cross Section	18
3.2 Detector Efficiency	21
3.3 Solid Angle of Observation	22
3.4 Computer Program	22
3.5 Results of Computation	26
4.0 CONTROL OF SPURIOUS BACKGROUND	31
5.0 EXPERIMENTAL RESULTS	39
6.0 THE POSSIBILITY OF USING CHARACTERISTIC X-RAYS TO DETERMINE GAS COMPOSITION	57
6.1 Carbon K Radiation ( $44\text{\AA}$ )	57
6.2 Oxygen K Radiation ( $23.6\text{\AA}$ )	61
7.0 CONCLUSIONS	64
7.1 Composition Sensitivity of Brems- strahlung Gauge	64
7.2 Ultimate Pressure Limits	66
7.3 The Possibility of Using K X-rays in the Determination of Gas Composition	68
7.4 The Possibility of Determining Hydrogen Concentrations Using the Bremsstrahlung Technique	68

## TABLE OF CONTENTS (Continued)

	Page
7.5 Advantages of the Bremsstrahlung Gauge	69
7.6 A Technique for Increasing Gauge Sensitivity	72
BIBLIOGRAPHY	77

## LIST OF TABLES

Table No.		Page
I	$\bar{Z}$ and $\bar{A}$ FOR REPRESENTATIVE GAS MIXTURES	25
II	CALCULATED X-RAY YIELDS	28
III	EXPERIMENTAL CONDITIONS	41
IV	GAS COMPOSITION SENSITIVITY	67

LIST OF FIGURES

Figure No.		Page
2-1	VACUUM SYSTEM BLOCK DIAGRAM	6
2-2	VACUUM CHAMBER DETAIL	9
2-3	ELECTRON GUN BIAS AND CONTROL UNIT	11
2-4	INDICATOR UNIT	13
2-5	CHARGE SENSITIVE PREAMP SCHEMATIC	15
3-1	VACUUM CHAMBER DETAIL A - GEOMETRY USED IN COMPUTER CALCULATION	27
3-2	X-RAY YIELD VS. ELECTRON ENERGY	30
4-1	FRACTION OF ELECTRONS BACKSCATTERED (WITH INCIDENT BEAM NORMAL TO SURFACE) AS A FUNCTION OF TARGET ATOMIC NUMBER	35
5-1	Fe <sup>55</sup> CALIBRATION SPECTRUM	40
5-2	VACUUM CHAMBER DETAIL B - SOURCE POSI- TIONS IN BACKGROUND MEASUREMENT	42
5-3	TYPICAL MEASURED BREMSSTRAHLUNG SPECTRUM	43
5-4	COMPUTED SPECTRUM FOR AIR AT T <sub>0</sub> = 10 kev (P-10 COUNTER FILL)	44
5-5	COMPUTED SPECTRUM FOR AIR AT T <sub>0</sub> = 10 kev, CORRECTED FOR ESCAPE PEAK OF ARGON IN P-10 FILL	45
5-6	DYNAMIC RESPONSE OF GAUGE (NO COLLIMATOR)	49
5-7	VACUUM CHAMBER DETAIL C - EXPERIMENTAL GEOMETRY WITH 0.25" COLLIMATOR	50

## LIST OF FIGURES (Continued)

Figure No.		Page
5-8	VACUUM CHAMBER DETAIL D-EXPERIMENTAL GEOMETRY WITH NO COLLIMATOR	47
5-9	MEASURED RESPONSE USING 0.25" DIAMETER COLLIMATOR	52
5-10	MEASURED RESPONSE WITH AND WITHOUT LIQUID NITROGEN (0.25" DIAMETER COLLIMATOR)	54
6-1	COUNTER EFFICIENCY VS. ENERGY (POLYPROPYLENE WINDOW)	60
6-2	COUNTER EFFICIENCY VS. ENERGY (MYLAR WINDOW)	62
7-1	OPERATING RANGES AND ERRORS OF VACUUM GAUGES	71
7-2	COLLECTOR SCHEMES TO REDUCE BACKGROUND	73

## 1.0 INTRODUCTION

Accurate density and pressure measurements in the region of medium to high vacua ( $10^{-3}$  -  $10^{-8}$  Torr) present a variety of problems. Normally, an investigator relies on elaborate ion gauge calibrations which are ultimately referred to McLeod gauge measurements, at pressures near  $10^{-3}$  Torr. Nonlinearity of ion gauge response makes extrapolation from the  $10^{-3}$  -  $10^{-4}$  Torr region extremely difficult. Ion gauges possess two additional shortcomings: The first arises from the difficulty in predicting gauge sensitivity as a function of gas composition. Ion gauge "pumping" imposes the second limitation; a measurement made with an ion gauge determines pressure in a region where considerable perturbation exists due to the presence of the measurement probe.

In order to surmount some of these measurement problems, we undertook a theoretical and experimental program to establish the feasibility of density (and hence pressure) measurements at low pressures by means of a relatively novel (Ref. 1) yet straightforward approach. The technique consists of observing the soft X-ray radiation produced when gases are bombarded by monoenergetic electrons in the 5 to 20 keV energy range. We considered both continuum X-ray production (thin target bremsstrahlung) and characteristic K $\alpha$  emission. The continuum X-ray yield measures a composition

averaged density; the intensity of characteristic radiation (e.g. the carbon  $K\alpha$  line at  $44\text{\AA}$ ) reveals elemental densities. We can deduce pressure from these density measurements if suitable assumptions are made regarding the chemical state of the gas.

In the analysis of the bremsstrahlung production process, we used the Sommerfeld Theory (Ref. 2) as extended for computer calculation by Berger (Ref. 3). This non-relativistic theory neglects orbital electron screening of the nuclear charge.

We used a computer program, developed under a related contract\*\*, and based on Berger's numerical tables (Ref. 4). The program first calculates  $I(\nu, \theta)$  where  $I(\nu, \theta)$  is the number of photons emitted per nucleus per frequency per interval per steradian at angle  $\theta$  to the electron beam direction. We then compute the anticipated count rate per nucleus by integrating over  $\nu$  and  $\theta$ . The integration over  $\nu$  includes the variation of counter efficiency with photon energy, while the  $\theta$  integration includes variations of counter solid angle along the electron beam path.

Input parameters such as solid angle, detector efficiencies and angle of observation were defined by the experimental facilities at our disposal. We considered both argon and krypton proportional counters having 0.5" diameter,

---

\*\* Air Force Contract No. F19(628)-67-C-0278

0.002" thick beryllium end windows. Typical counter solid angles were  $10^{-2}$  -  $10^{-3}$  steradians.

Using suitably weighted values of atomic number and atomic weight, we then computed expected count rates per mA per gm per cc of residual gas for several typical gas compositions.

As a result of our analysis we reached the following conclusions:

- (1) Over the electron energy range of 5 to 10 kev, the count rate per mA per gm per cc varies by less than 10%. Thus a relatively inexpensive electron beam power supply suffices.
- (2) The X-ray yield is proportional to density and varies linearly with Z.
- (3) The X-ray yield directly measures pressure (defined as a mechanical quantity) only if the chemical composition of the gas molecules is known. For example, at a given pressure and temperature, X-ray yields from monatomic, diatomic and triatomic oxygen vary as the ratio of molecular weights, i.e. 1:2:3.
- (4) Spurious background count rates and the time available for an observation determine the minimum density and pressure that can be measured. For a 10 mA electron beam and a counter solid angle of 0.1

steradian, a density of  $5 \times 10^{-15}$  gm/cm<sup>3</sup> will produce a count rate of one per second. For diatomic nitrogen, this density corresponds to a pressure of  $3 \times 10^{-9}$  Torr at 20°C. If the background arises solely from cosmic rays (1 per minute) then an observation time of 100 seconds yields a measurement accurate to 10%, in the absence of instrumental errors.

We undertook a program of laboratory measurements to verify some of the above predictions. In addition, we investigated, both experimentally and analytically, the problem of spurious X-ray background. This study resulted in design guidelines for a prototype gauge.

Finally, we explored the feasibility of using characteristic X-rays to determine gas composition. The main problem, when using electron excitation, arises from the continuous bremsstrahlung background. Using spectrally selective counter windows (e.g. a polypropylene window for observation of the carbon line at  $44\overset{\circ}{\text{A}}$ ), band-width/insertion-loss tradeoff calculations allowed us to determine signal to noise ratios. For a 12  $\mu\text{m}$  polypropylene detector window, a typical signal to noise ratio was  $7.75 \times 10^{-2}$ . The low characteristic X-ray yield results from the unfavorable competition with Auger electron production typical of light elements. Thus, we conclude this technique is impractical.

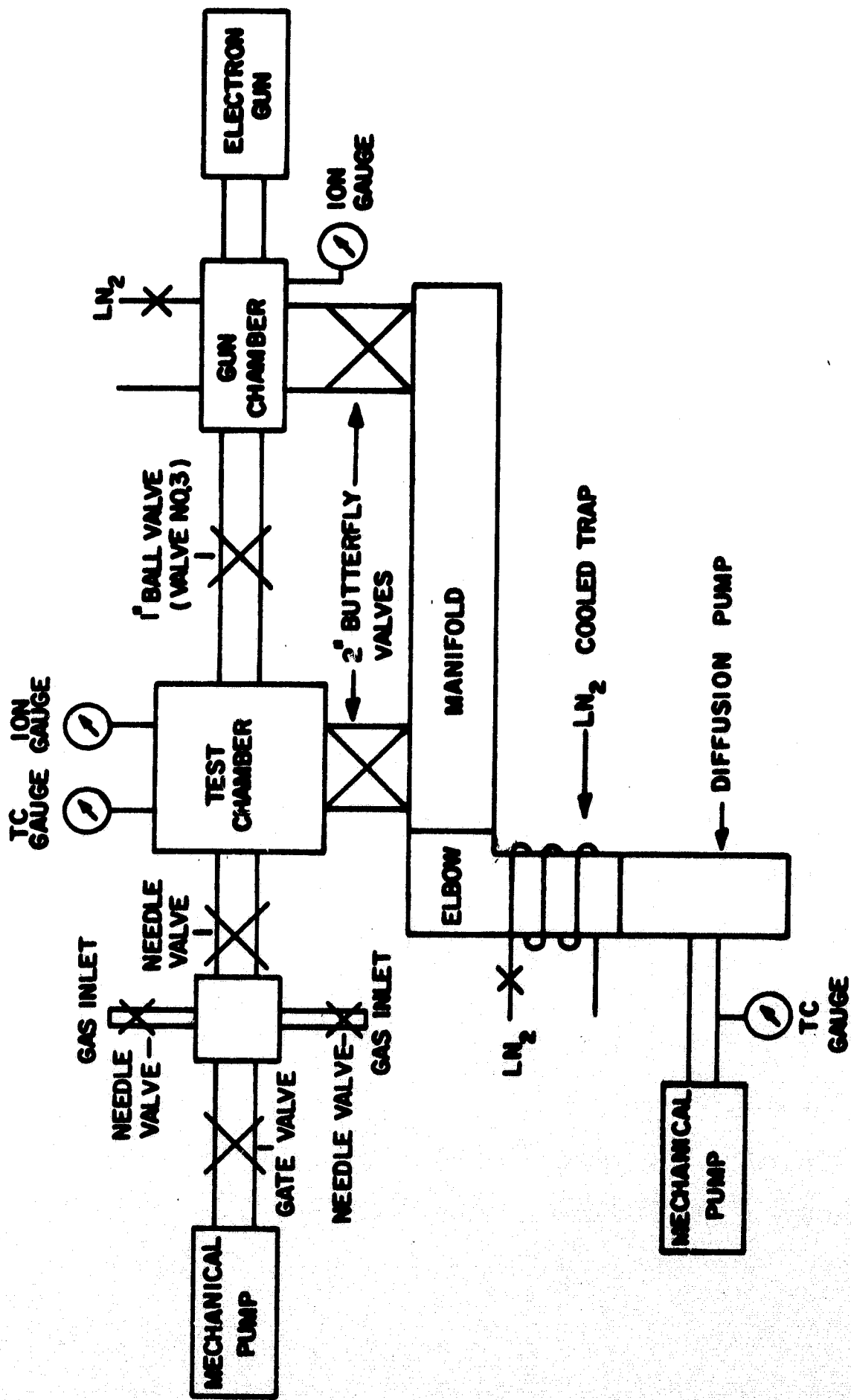
## 2.0 EXPERIMENTAL ARRANGEMENT

### 2.1 Vacuum System

Figure 2-1 illustrates the vacuum system in block diagram form. An 800 liter per second diffusion pump and a 425 liter per minute mechanical pump evacuate the manifold through a liquid nitrogen cooled elbow. This elbow pumps water vapor and provides a trap for back streaming oil. Diffusion pump foreline pressure is monitored by a thermocouple gauge. Two-inch butterfly valves isolate the manifold from the test and gun chambers. An additional 150 liter per minute mechanical pump functions as a roughing pump for the two chambers. This arrangement also permits the diffusion pump to operate while the chambers are open to air.

The roughing line contains a one-inch cross with two gas inlets and needle valves. An additional needle valve between test chamber and cross allows fine adjustment of chamber pressure. A good quality, one-inch, globe water valve isolates the roughing pump from the cross when desired.

The electron gun chamber contains the gun mount, ion gauge port, and viewing port. A one-inch ball valve provides isolation from the test volume. The liquid nitrogen cooled casing of the gun chamber pumps water vapor.



VACUUM SYSTEM BLOCK DIAGRAM

FIG. 2-1

A variety of electron guns are adaptable to the system. We used a Griffiths Electronics Model GE-63 mounted in a standard one-inch I.D. glass tube, five and one-quarter inches long. GC Electronics TV Tube Coat, painted on the inside and also on the open end of the tube, provides a ground return for the third and fifth grids. An eight pin male plug at the base mates with the control cable.

The gun mount allows two degrees of freedom each in translation and rotation and also maintains a vacuum seal. A standard one and one-quarter inch vacuum coupling, held in a gimbal arrangement, provides electrical and vacuum interfaces with the glass tube. A thin stainless steel bellows mates the coupling with a flange seal on the titanium pump. The gimbals mount inside a stainless steel cylinder welded to a movable plate. A screw arrangement, permitting lateral movement, mounts the plate to the flange. Four screws, threaded through the cylinder, bear against the glass tube and provide the two degrees of freedom in rotation. Manipulating both sets of screws allows beam centering through the tubulation and into the Faraday cup.

Ion gauge and viewing ports complete the gun chamber. At  $10^{-4}$  Torr the beam is faintly visible in the viewing port, facilitating rough gun alignment.

The test chamber contains a Faraday cup, ion and thermocouple gauge ports and detector and exhaust ports. A

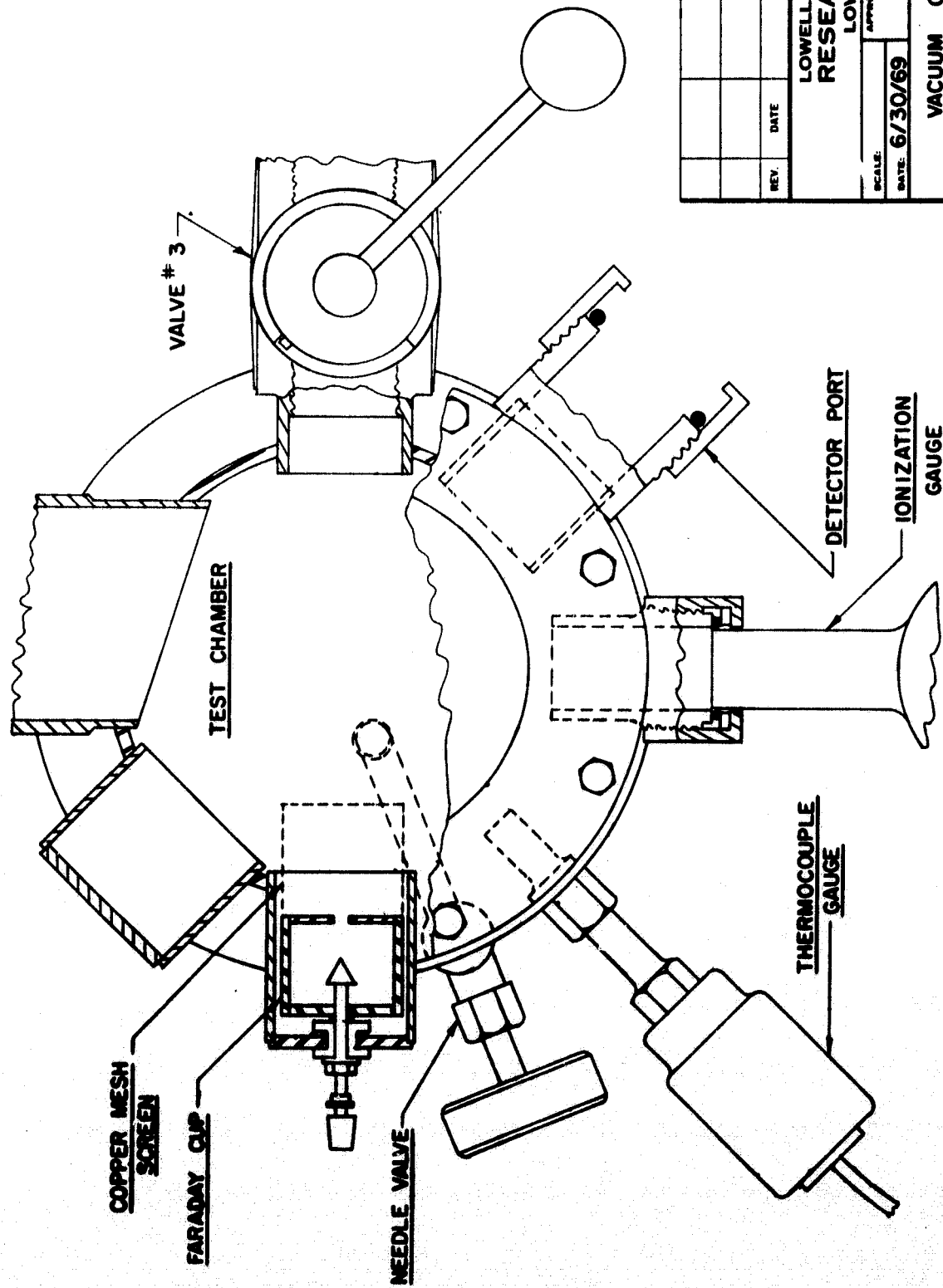
one-half inch thick Plexiglass cover allows visual monitoring. GC TV Tube Coat completely covers the inside of the chamber to minimize wall fluorescence. Figure 2-2 illustrates this section in detail.

A nine liter liquid nitrogen reservoir, vented to atmospheric pressure, mounts to the system through a wood framework. Separate valves and tubulation are used for each cooling coil. This container must be replenished from a large capacity tank approximately every 45 minutes.

## 2.2 Electronics Rack

This assembly provides bias and control voltages for the electron gun and also monitors beam current collected by the Faraday cup. The rack contains an Electron Gun Bias and Control Unit, an Indicator Unit, a Spellman PN-30 high voltage power supply, and a twelve volt automobile storage battery.

We have already described the gun's physical characteristics in the previous section. Connections to the heater, cathode, control grid, accelerator grid, and focus ring run through a five conductor shielded cable. Each conductor consists of 18 gauge wire covered by 50 kilovolt DC rated insulation. Aluminum zipper tubing provides an easily installed outer shield which must be grounded to allow safe handling. Safety is essential since all gun elements operate at or near the negative high voltage potential.



REV.	DATE	DESC. OF CHG.	DR. BY	APP'D. BY
LOWELL TECHNOLOGICAL INSTITUTE RESEARCH FOUNDATION LOWELL, MASSACHUSETTS				
APPROVED BY			DESIGNED BY	HGR
DATE: 6/30/69			CHECKED BY	
VACUUM CHAMBER DETAIL				
PROJECT NO.	DECIMAL DIMENSIONS ± .005			DRAWING NUMBER
1906-R	FRACTIONAL DIMENSIONS ± 1/64"			
UNLESS OTHERWISE SPECIFIED.				200431

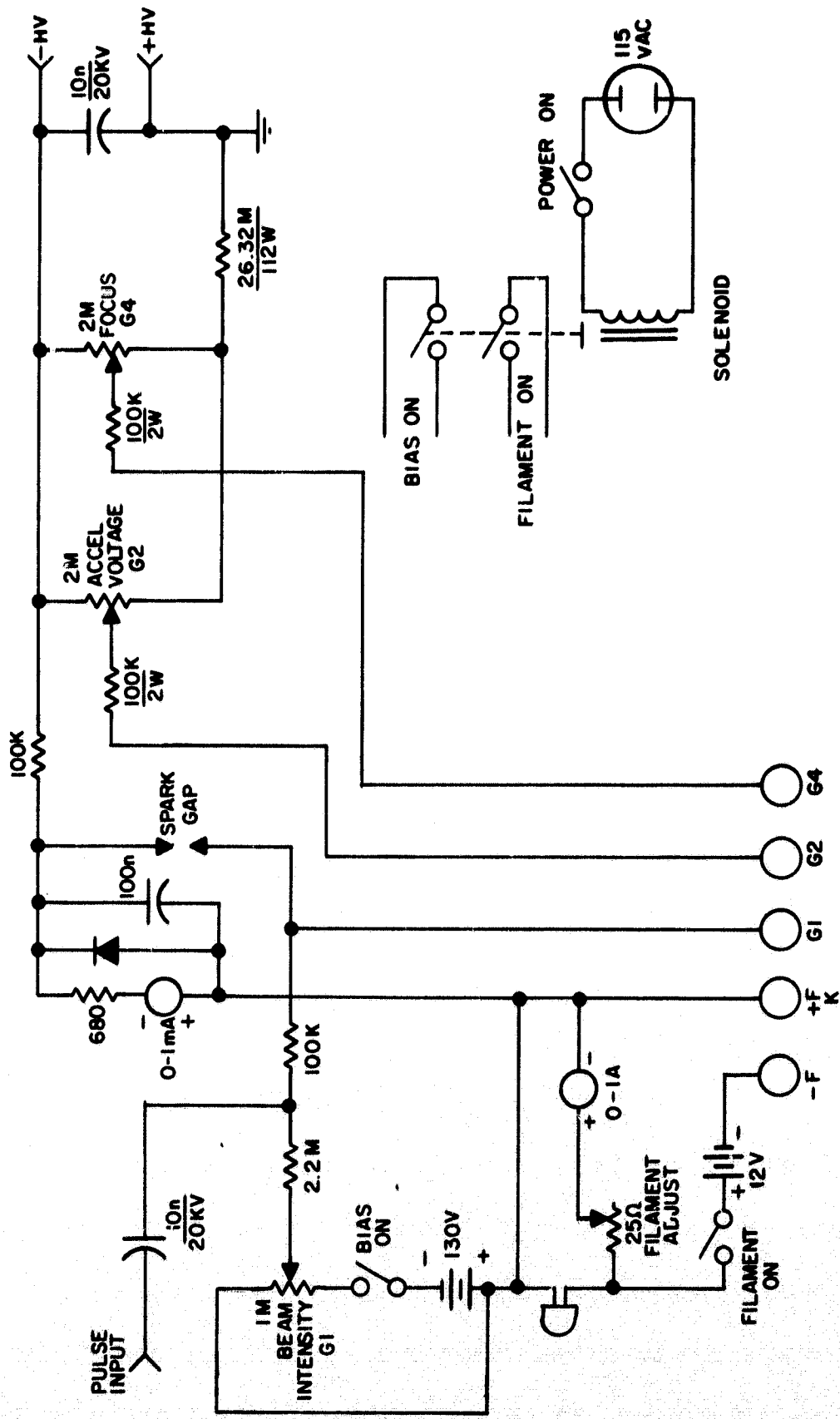
VACUUM CHAMBER DETAIL  
FIG. 2-2

Gun operation is controlled by the Electron Gun Bias and Control Unit. Figure 2-3 (drawing number 100851) shows the circuitry. Filament current is adjusted by a rheostat and monitored on a one ampere AC meter. A dry battery (radio "B" battery) and a potentiometer supply variable control grid bias from zero to minus 130 volts. This, in conjunction with the accelerator voltage, controls the flow of cathode current. A one milliamper DC meter monitors cathode current.

The positive high voltage connects to system ground. Negative potential is applied to a bank of 56, 470K, two watt resistors acting as a bleeder and providing one arm of a voltage divider. A pair of parallel connected two megohm potentiometers make up the other arm. The wiper of one potentiometer supplies accelerator voltage and the other supplies focus voltage.

A solenoid, operating from the AC line, turns on the bias and filament voltages. The solenoid plunger operates a DPST snap-acting switch through a nylon cord, since negative high voltage is present on all components.

The main chassis for the control unit is a piece of three-eighths inch plywood and a sheet of Plexiglass on which are mounted the meters, controls, and resistor bank. Angle brackets mount this assembly to a rack panel. All controls use Plexiglass couplings to the panel.



ELECTRON GUN BIAS AND CONTROL UNIT

FIG. 2-3

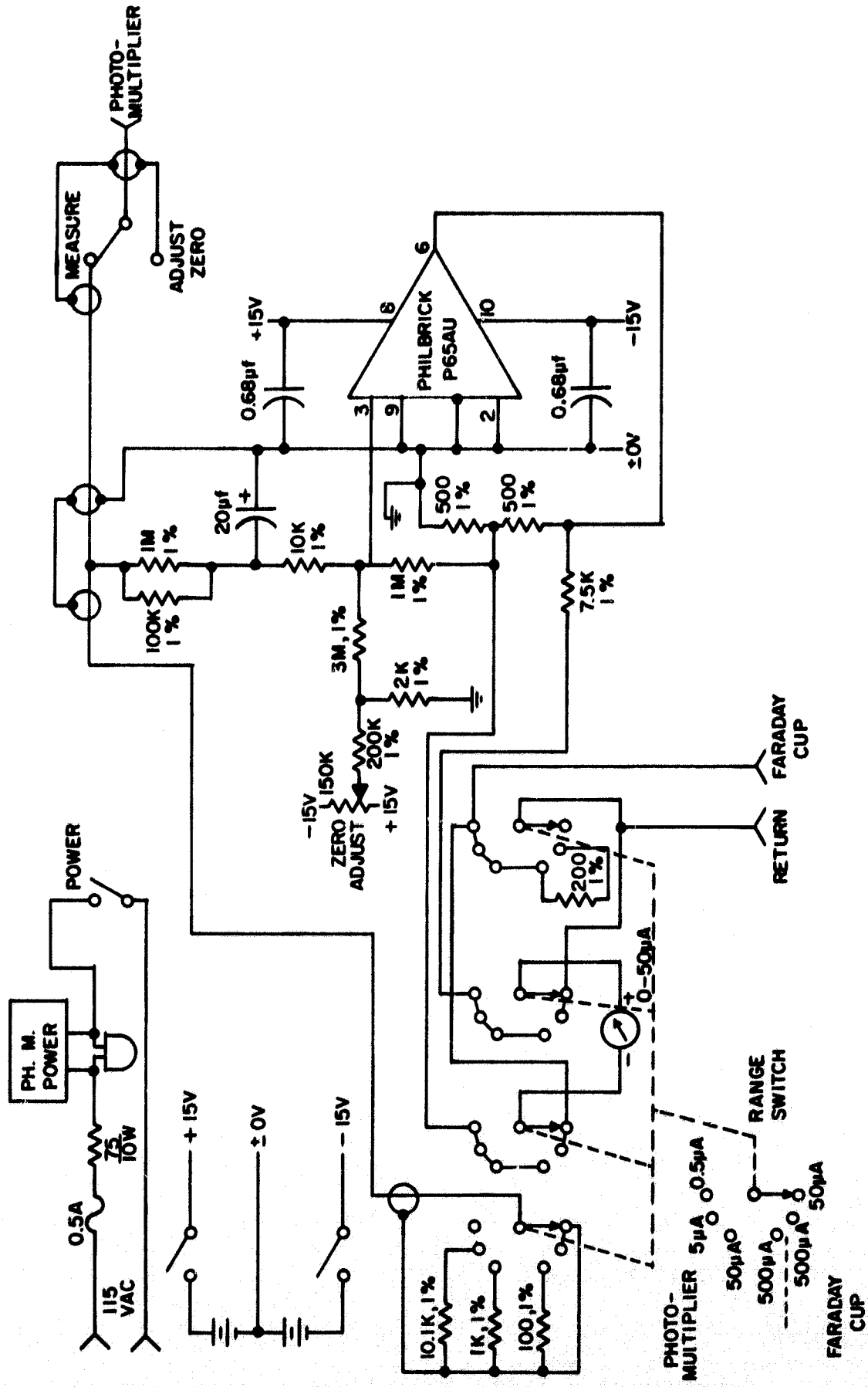
A 95 ampere-hour car battery powers the gun filament. Since negative high voltage appears on the terminals it must be insulated from the rack. A satisfactory installation results by placing a few inches of polystyrene foam on the rack floor and resting the battery in this location.

We used a high voltage supply capable of 30 kilovolts at two milliamperes but ten to twenty kilovolts at one milliampere would be sufficient. Voltage regulation of 0.1% would ease some experimental difficulties.

The Indicator Unit measures the beam current collected by the Faraday cup. Figure 2-4 (drawing number 100850) shows the circuitry. A Philbrick P65AU solid state operational amplifier and a 50 microamp DC meter provide full scale ranges of 0.5 to 500 microamps. Two fifteen volt dry batteries power the operational amplifier. We used this amplifier with its sensitive response, to monitor Faraday cup current. The most sensitive scale aids initial gun alignment.

### 2.3 Detection

X-ray detection requires a charge-sensitive preamplifier, a monitor scope, multi-channel analyzer, and most any unsophisticated event or frequency counter. A proportional counter, producing a charge pulse for each incident X-ray, is mounted through a port in the test chamber. The preamplifier shapes the input pulse and produces a voltage output to drive the analyzer.



INDICATOR UNIT  
FIG. 2 - 4

The charge sensitive preamplifier uses a commercial wide-band integrated circuit (IC) to obtain small size, reduced circuit complexity, and predictable performance. The circuit configuration, shown schematically in Figure 2-5 makes the output voltage proportional to the input charge.  $C_f$  and  $C_s$  determine the charge sensitivity of the preamplifier. The other components provide dc-biasing, stabilization, and protection.

$C_f$ ,  $R_f$ ,  $C_s$ ,  $R_s$ , and  $R_{DC}$  form a frequency-independent feedback network (above a few hundred kHz) permitting the 51 pf lead capacitor between pins 5 and 6 to stabilize the amplifier and allow 40 dB of closed-loop gain with about 45° of phase margin. The measured phase margin at 0 dB loop gain was about 40°. Maximum bandwidth capabilities are realized from the operational amplifier by using lead-compensation only.

Closed-loop bandwidth of this amplifier is about 9 MHz (-3 dB) resulting in a 40 nsec rise time ( $\tau_r = \frac{.35}{BW}$ ). The fall time, defined ( $t_f = 2.2 \tau_f$ ) by the time constants  $C_f$ ,  $R_f$  and  $C_s$ ,  $R_{DC}$ , equals 3.1  $\mu$ sec.

Since the input pulse rise time is 125 nsec, corresponding to a bandwidth of 3 MHz, the open-loop gain and the closed-loop gain of the amplifier will be given at this frequency. The loop gain of the preamplifier is about 15 dB with an expected variation of  $\pm 5$  dB for the distribution of  $\mu A702C$ 's. The tolerances of the feedback capacitors plus



the loop gain causes a worst-case gain variation from unit-to-unit of  $\pm 20\%$ .

The closed-loop gain of the preamplifier is given by:

$$\frac{e_o}{Q_i} = \frac{A}{C_s + C_f(1+A)} \text{ (volts/coulomb)}$$

where  $A$  = open-loop gain,  $Q_i$  = input charge and  $e_o$  = output voltage. For the open-loop gains in this circuit,  $e_o/Q_i$  is most sensitive to changes in  $C_f$  and  $A$ . For a low-gain  $\mu A702C$ , with  $\frac{\Delta C_f}{C_f} = \pm 200$  ppm and  $\frac{\Delta C_s}{C_s} = 0$  to  $+70$  ppm, the gain stability from  $0$  to  $+50^\circ C$  is  $+1.5\%$ ,  $-2.4\%$ . Using an NPO capacitor for  $C_s$  and a  $300$  ppm negative temperature coefficient capacitor for  $C_f$  will yield stabilities of  $+0.39\%$ ,  $-0.9\%$ .

The 1N4148 diodes protect against large, possibly destructive, input voltages. Arcing in the counter tube could otherwise destroy the preamplifier. An additional  $100$  ohm resistor and shunt diode render these occasional transients harmless.

The output is transformer-coupled to prevent transmitting the offset voltage of the preamplifier. Since the output returns to the zero reference, a  $100$  ohm series resistor limits the current drawn through the IC output transistor by the dc offset voltage.

### 3.0 SYSTEM ANALYSIS

We wish to establish the relationship between X-ray count rate and mass density of the residual gases under study. Input parameters should include a specification of gas composition, detector-electron beam geometry, proportional counter efficiency, electron beam current and voltage. We first define the differential bremsstrahlung cross section,  $\frac{d\sigma}{d\Omega dE}$  as the number of photons produced per second per unit photon energy increment per unit solid angle per incident electron per target atom per  $\text{cm}^2$ .  $\frac{d\sigma}{d\Omega dE}$  is a function of electron energy  $T_0$ , photon energy  $E$ , atomic number of the target atom,  $Z$  and the angle of observation,  $\theta$ , where  $\theta$  is measured relative to the electron beam direction. If the counter has an efficiency  $\epsilon(E)$  and subtends a solid angle  $\Omega(\theta)$  with respect to point  $X$  along the electron beam path, then the number of X-rays produced per electron per atom per  $\text{cm}^3$  is given by

$$Y_A = \int_{E_1}^{E_2} \int_{X_1}^{X_2} \frac{d\sigma}{dE d\Omega} \cdot \epsilon(E) \cdot \frac{d\Omega}{dX} dX dE$$

$X_1$  and  $X_2$  are defined by the detector field of view;  $E_2$  equals  $T_0$ , the electron energy and  $E_1$  is defined by the long wavelength cut-off of the counter. Then, if there are  $n_a$  atoms per  $\text{cm}^3$  and an electron current of  $i$  (mA), the total yield  $Y_T$  is given by

$$Y_T = K i n_a \iint \frac{d\sigma}{d\Omega dE} \cdot \epsilon(E) dE \frac{d\Omega}{dX} dX \text{ cps}$$

where

$$K = 6.25 \times 10^{15} \frac{\text{electrons}}{\text{sec} \cdot \text{mA}}$$

This formula is correct under the assumption that both electron and X-ray attenuation by the residual gases in the system is negligible. The stopping power of air for a 10 kev electron is  $20 \frac{\text{Mev}}{\text{gm/cm}^2}$ . At a pressure of  $10^{-3}$  Torr, a 10 kev electron loses only 0.3 ev over a 10 cm path length; at the same pressure, a 1 kev X-ray has a mean free path of 2 km. Clearly absorption is negligible at these pressures.

Now,  $n_a = \frac{N_0}{A} \rho$  where  $A$  is the atomic weight of the gas under study,  $N_0$  is Avogadro's number and  $\rho$  is the mass density in gm/cc.

Then

$$Y_T = K i Y_A \frac{N_0 \rho}{A}$$

and we can see that the total count rate is proportional to the mass density. The determination of  $\frac{d\sigma}{d\Omega dE}$  will now be considered.

### 3.1 The Bremsstrahlung Cross Section

We consider first  $\frac{d\sigma}{dE}$ , the differential bremsstrahlung cross section integrated over angle. The simplest formulation is that described by Evans (Ref. 5, pg. 603), for

the case of non-relativistic electrons interacting with a nucleus of charge  $Z$ . The effect of atomic electron screening is ignored.

Thus

$$\frac{d\sigma}{dE} = \sigma_0 B Z^2 \left( \frac{T_0 + m_0 c^2}{T_0} \right) \frac{1}{E} \frac{\text{cm}^2}{\text{nucleus} \cdot \text{kev}}$$

where

$m_0 c^2$  = rest energy of the electron

$T_0$  = kinetic energy of incident electron

$B$  = a slowly varying function of  $T_0$  and  $Z$ , having a value between 5 and 20

$E$  = photon energy (kev)  $\leq E_{\text{max}} = h\nu_{\text{max}} = T_0$

$\sigma_0 = \frac{1}{137} \frac{e^2}{m_0 c^2} = 0.58 \text{ millibarn/nucleus}$

We see that the cross section depends on the nuclear species primarily through the  $Z^2$  term.

Since we would like to calculate the expected X-ray yields as accurately as possible, we have developed our analysis using the bremsstrahlung theory of Sommerfeld (Ref. 2), as later extended for computer calculation by Berger (Ref. 4-5). The resulting cross sections exhibit a functional dependence on  $Z$ ,  $T_0$ , and  $E$  which is similar to that predicted by Evans' formula; the higher order variations contained in  $B$ , are automatically accounted for.

The Sommerfeld theory is basically a Distorted Wave Born Approximation (DWBA) where unbound coulomb wave functions describe the incoming and outgoing electron. The theory is non-relativistic and screening is ignored.

Using Berger's terminology,

$$W_s = A dv \left\{ \left( \frac{Z}{a} \right)^2 \frac{1}{(e^{2\pi\alpha} - 1)(1 - e^{-2\pi\beta})} \frac{X_o}{K_1^2} \frac{d}{dX_o} |F(X_o)|^2 \right\}$$

Where  $W_s$  = total energy radiated in energy range  $d(h\nu)$  by an electron of velocity  $V_1$  incident on one atom per  $\text{cm}^2$  of atomic number  $Z$ . The electron has velocity  $V_2$  after the interaction.

$$K_1 = \frac{mV_1}{\hbar} \quad a = \frac{\hbar^2}{m_0 e^2} \quad \alpha = \frac{Z}{K_1 a}$$

and

$$\beta = \frac{Z}{K_2 a} \quad \text{where } K_2 = \frac{mV_2}{\hbar}$$

also

$$X_o = \frac{4\alpha\beta}{(\beta-\alpha)^2} \quad A = \frac{8\pi}{3} \frac{e^2}{C^3} \frac{h^2}{m_0^2} = 3.794 \times 10^{-48} \text{ erg cm}^2 \text{ sec.}$$

$F(X_o)$  is a hypergeometric function. Berger calculated  $F(X_o)$  over a wide range of  $\alpha$  and  $\beta$ . This resulted in a computer print out of intensity,  $W_s$ , as a function of  $\beta$  and  $\alpha$ .  $W_s$  is related to  $\frac{d\sigma}{dE}$  by the relation

$$\frac{d\sigma}{dE} = \frac{W_s}{E dE}$$

where  $E$  is the photon energy in ergs. Thus  $\frac{d\sigma}{dE}$  can be obtained

from Berger's computer print out for a given value of  $\alpha$  and a range of  $\beta$ .  $\alpha$  and  $\beta$  are related to  $T_0$ , incident electron energy, and  $E$ , the outgoing photon energy by the relations:

$$\alpha = \frac{0.116642Z}{\sqrt{T_0}} \quad \beta = \frac{0.116642Z}{\sqrt{T_0 - E}}$$

For a given  $\alpha$ ,  $\beta$  is allowed to vary in the range defined by  $0.1T_0 < E < T_0$ . Using the formulation of Kirkpatrick and Wiedman (Ref. 6), we find

$$\frac{d\sigma}{d\Omega dE} \left( \frac{\text{cm}^2}{\text{ster} \cdot \text{kev}} \right) = \frac{6}{\pi} \times 10^{-10} \frac{d\sigma}{dE} (1+2D)^{-1} [\sin^2\theta + D(1+\cos^2\theta)]$$

where  $D$  is Sommerfeld's depolarization factor given by

$$D = \left[ \frac{\alpha^2 + \beta^2}{2\alpha\beta} \ln \frac{\alpha + \beta}{\alpha - \beta} - 1 \right] \left[ 2 \left\{ \frac{\beta^2 - \alpha^2}{2\alpha\beta} \ln \left( \frac{\alpha + \beta}{\alpha - \beta} \right) + 1 \right\} \right]^{-1}$$

### 3.2 Detector Efficiency

For the case of an ideal counter, the product of window transmission and gas absorption yields the efficiency  $\epsilon(E)$ .

$$\epsilon(E) = e^{-\mu_w t_w} (1 - e^{-\mu_g t_g})$$

where  $\mu_w$  and  $\mu_g$  are the linear absorption coefficients of the counter window and gas respectively;  $t_w$  and  $t_g$  are the thicknesses of window and gas respectively.

We considered two different detectors. Both were cylindrical proportional counters having 0.5 inch diameter, 0.002" thick beryllium end windows and an active counting gas

depth of 0.5 inch. One was filled with 90% krypton and 10% CO<sub>2</sub>, at a total pressure of 1 atmosphere; the other contained a standard P-10 mixture (90% Ar and 10% CH<sub>4</sub>) at atmospheric pressure. We obtained  $\frac{\mu}{\rho}$  values from Henke's (Ref. 14) work and incorporated the Ar and Kr absorption edges at 3.2 and 14.35 kev respectively.

### 3.3 Solid Angle of Observation

The calculation of solid angle subtended by the detector at a point X along the electron beam path divides into two parts; the solid angle  $\Omega_0$  of the collimator and the reduction P in solid angle because the detector sees only part of the radiation entering the collimator. We obtained formulae for these factors from Reference 7 (R and D Design Evaluation; Density Measurement Rocket Payloads Using Bremsstrahlung).

### 3.4 Computer Program

We modified a computer program developed under a related contract (see Reference 7). The program calculates system response in counts per sec per mA of electron beam per gm per cc of target gas. The calculation was performed for several gas compositions and at electron energies, T<sub>0</sub>, of 5, 10, 15 and 20 kev. We now list the relevant input parameters.

## 1.) Cross Section Calculations

$T_0$ ,  $\alpha$ , and  $\bar{Z}$ ; a table of  $W_s$  vs  $\beta$  for given  $\alpha$  values.

$\bar{Z}$  is a suitable average of elemental atomic numbers. We determined it in the following way.

To first order.

$\frac{d\sigma}{d\Omega dE} \propto Z^2$  for the case of a single element. Then

for a mixture of gases, the average cross section is

$$\frac{\bar{d\sigma}}{d\Omega dE} \propto \sum_i \frac{N_i}{N} Z_i^2$$

where  $N_i$  and  $Z_i$  are the number density and nuclear charge of the  $i^{\text{th}}$  elemental species. We then use  $Z^2 = \sum \frac{N_i}{N} Z_i^2$ , along with  $T_0$ , to specify the appropriate  $\alpha$  and hence the  $W_s$  and  $\beta$  values.

$$N_i = \sum_k \frac{N_0}{A_k} \cdot \rho_k \cdot n_{ki} ;$$

where

$N_0$  = Avogadro's Number =  $6.02 \times 10^{23}$  molecules per mole

$A_k$  = Molecular weight of  $k^{\text{th}}$  molecular species

$\rho_k$  = density of  $k^{\text{th}}$  molecular species

$n_{ki}$  = no. of  $i^{\text{th}}$  species atoms in the  $k^{\text{th}}$  species of molecule

and

$$N = \sum_i N_i = \sum_{ij} \frac{N_0}{A_j} \rho_j n_{ji} ,$$

Hence

$$\bar{Z} = \frac{\sum_{ik} \frac{\rho_k}{A_k} n_{ki} Z_i^2}{\sum_{ij} \frac{\rho_j n_{ji}}{A_j}}$$

But, for an ideal gas  $\rho_k \propto A_k P_k$  where  $P_k$  is the partial pressure of the  $k^{\text{th}}$  molecular species. Then

$$\bar{Z}^2 = \frac{\sum_{ik} (P_k n_{ki}) Z_i^2}{\sum_{ik} (P_k n_{ki})}$$

Similarly, we showed that  $\bar{A}$ , the average atomic weight in a composite gas is given by

$$\bar{A} = \frac{\sum_{ik} (P_k n_{ki}) A_i}{\sum_{ik} (P_k n_{ki})}$$

We calculated  $\bar{Z}$  and  $\bar{A}$  for the gas compositions shown in Table I. In addition to air and hydrogen, we considered two compositions typical of residual gases in vacuum systems evacuated by an oil diffusion pump and mercury diffusion pump respectively; liquid nitrogen traps are used in both cases. The analyses were tabulated by Dushman (Ref. 8, pg. 208). We chose dibutyl phthalate [ $C_6 H_4 (COOC_4 H_9)_2$ ] as a typical pump oil.

## 2.) Counter Efficiency

Input data included the window and counting gas thickness in  $mg/cm^2$  and a table of  $\frac{\mu}{\rho}$  vs.  $E$  over the energy range of interest (Ref. 14).

TABLE I

 $\bar{Z}$  AND  $\bar{A}$  FOR REPRESENTATIVE GAS MIXTURES

Residual Mixture	Air	Pure H <sub>2</sub>	Oil Diffusion & -78°C Trap	Hg Diffusion Pump & -78°C Trap
$\bar{Z}$	7.3108	1	4.566	71.526
$\bar{A}$	14.55	1.008	6.6401	161.816
Gas	% by Volume	Partial Pressure %	Partial Pressure %	Partial Pressure %
H <sub>2</sub>		100.00	16	—
N <sub>2</sub>	78.084	—	—	—
O <sub>2</sub>	20.947	—	—	—
Ar	0.934	—	—	—
CO	—	—	5.5	0.48
CO <sub>2</sub>	—	—	2.8	0.48
H <sub>2</sub> O	—	—	38.0	0.96
Air	—	—	8.8	—
Hg	—	—	—	97.5
Hydro-carbons C <sub>6</sub> H <sub>4</sub> (COOC <sub>4</sub> Hg) <sub>2</sub>	—	—	27.6	0.52

### 3.) Solid Angle

The following parameters were used to represent the laboratory situation; with reference to Figure 3-1

$\theta_0$  = angle between counter axis and electron beam direction =  $135^\circ$

$\theta_{\min}$  = minimum angle just outside detector field of view =  $122^\circ$

$\theta_{\max}$  = maximum angle just outside detector field of view =  $147^\circ$

Gamma = distance from collimator to electron beam along the detector axis = 3.75"

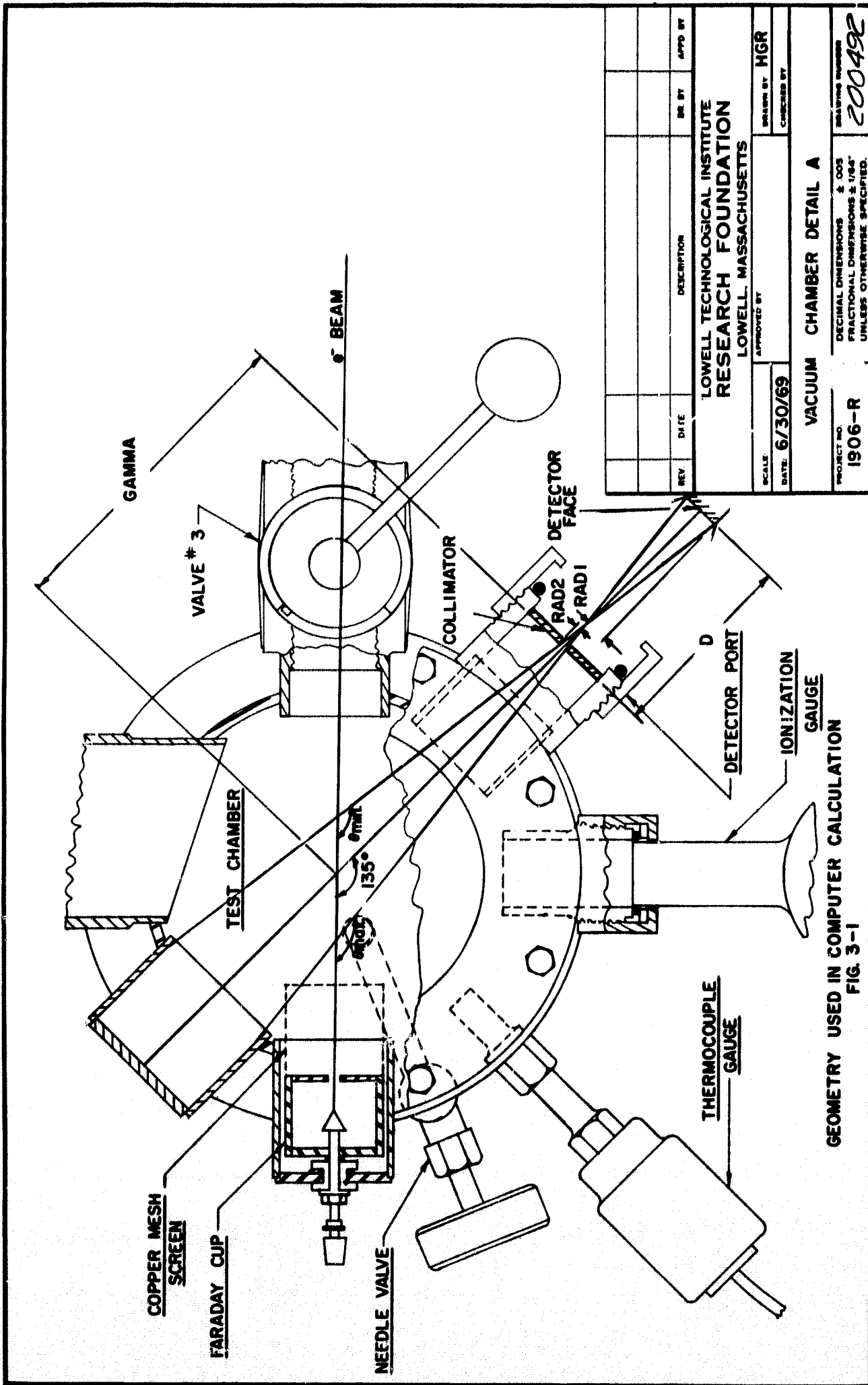
Rad 1 = radius of collimator = 0.1"

Rad 2 = radius of detector window = 0.25"

D = distance from collimator to detector window = 2.25"

### 3.5 Results of Computation

We list the results of 20 computer runs in Table II, and plot the variation of X-ray yield with electron energy in Figure 3-2. We can immediately estimate the ultimate pressure limits we can achieve with our laboratory set up. If we consider pure air, at  $20^\circ\text{C}$ , the density at 1 Torr pressure is  $1.5855 \times 10^{-6}$  gm/cm<sup>3</sup>. Now 0.5 mA is a reasonable beam current at 5 keV. Therefore, at a pressure of  $10^{-7}$  Torr, we obtain a count rate of  $1.81 \times 10^{12}$  cps/mA-gm per cc x 0.5 mA



GEOMETRY USED IN COMPUTER CALCULATION  
FIG. 3-1

REV.	DATE	DESCRIPTION	DR. BY	APPD. BY

LOWELL TECHNOLOGICAL INSTITUTE  
 RESEARCH FOUNDATION  
 LOWELL, MASSACHUSETTS

SCALE: DATE 6/30/69  
 APPROVED BY: HGR  
 CHECKED BY:

PROJECT NO. 1906-R  
 VACUUM CHAMBER DETAIL A  
 DRAWING NUMBER 200492  
 DECIMAL DIMENSIONS & ODS  
 FRACTIONAL DIMENSIONS & 1/64"  
 UNLESS OTHERWISE SPECIFIED.

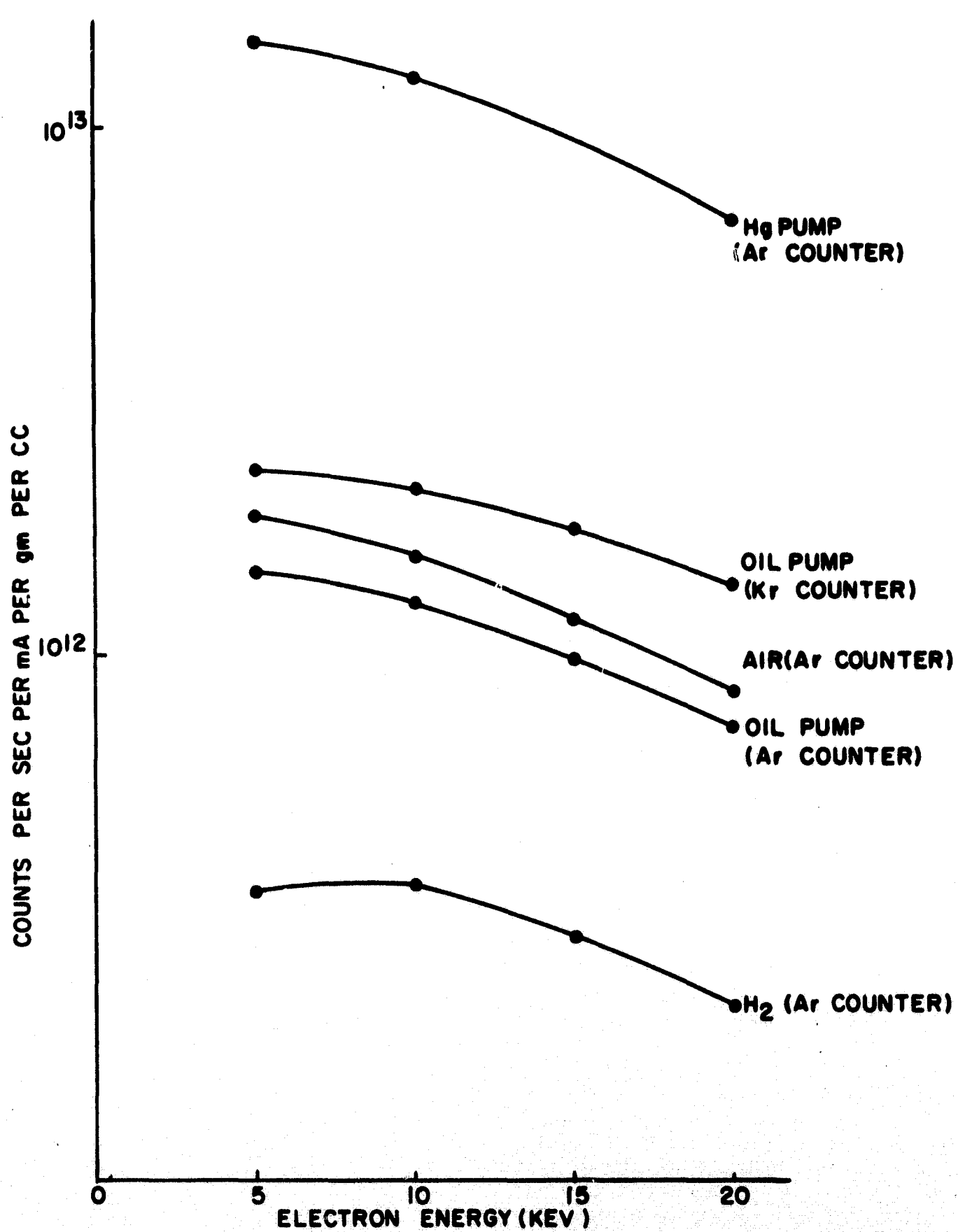
TABLE II  
 CALCULATED X-RAY YIELD  
 IN COUNTS PER SECOND PER MA PER GM PER CM<sup>3</sup>\*  
 MULTIPLY VALUES FROM TABLE BY 10<sup>12</sup>

T <sub>0</sub> (Electron Energy)	5 kev	10 kev	15 kev	20 kev
Conditions				
H <sub>2</sub> $\bar{A} = 1.008$ $\bar{Z} = 1$ Ar Counter	0.358	0.365	0.295	0.219
Air $\bar{A} = 14.55$ $\bar{Z} = 7.3108$ Ar Counter	1.81	1.54	1.17	0.853
Hg Pump & -78°C Trap $\bar{A} = 161.816$ $\bar{Z} = 71.526$ Ar Counter	14.4	12.1		6.63
Oil Pump & -78°C Trap $\bar{A} = 6.6401$ $\bar{Z} = 4.566$ Ar Counter	1.43	1.25	0.981	0.714
Oil Pump & -78°C Trap $\bar{A} = 6.6401$ $\bar{Z} = 4.566$ Kr Counter	2.22	2.08	1.71	1.35

\*Calculated for geometry defined in text - 0.1" Collimator  
 (See Figure 3-1)

$\times 1.5855 \times 10^{-7}$  gm/cc per Torr  $\times 10^{-7}$  Torr or 8.6 counts per minute.

Figure 3-2 also reveals that yield is quite insensitive to electron energy  $T_0$ , in the 5 to 10 kev range. The advantage of using a krypton counter, with its somewhat higher efficiency is also apparent.



X RAY YIELD VS ELECTRON ENERGY (CALCULATED)

FIG. 3-2

#### 4.0 CONTROL OF SPURIOUS BACKGROUND

We considered the following sources of spurious background:

- 1.) Cosmic rays
- 2.) Bremsstrahlung and characteristic X-ray production from electrons striking parts of the chamber in field of view of the detector.
- 3.) X-rays produced in the electron collector and which are seen directly by the detector.
- 4.) Secondary scattering of collector produced X-rays from parts of the chamber within the detector field of view.
- 5.) Secondary scattering of collector produced X-rays from residual gas atoms in the field of view of the detector.

An optimum gauge design should aim at a background level determined only by the local cosmic ray flux ( $1\sim 2$  per minute). As we shall see, such a goal is indeed feasible if we impose certain simple geometrical constraints on the gauge design.

Consider the electron beam; electrons impinging on the chamber walls within the detector field of view represent a prodigious source of background. The only solution is to eliminate them. Spurious electrons arise from the following mechanisms:

- 1.) Poor electron gun focussing, with considerable scattering from the exit electrode.

This effect should be negligible for a properly aligned electron gun and an appropriate choice of focus voltage.

- 2.) Secondary electron production within the beam collector. Application of a suitable positive potential (~100 volts) in series with the collector current meter will suppress secondary emission entirely.
- 3.) Deviation of the electron beam trajectory by local magnetic fields. When the magnetic field, H, is perpendicular to the initial beam direction

$$Y \approx \frac{X^2}{2\rho} \text{ for } \frac{Y}{X} \ll 1$$

where Y is the electron beam deflection at right angles to the initial beam direction, X is the distance from the electron gun exit to rear of collector cup, and  $\rho$  is the radius of curvature of the electron trajectory in magnetic field. For a 5 keV electron in a 0.5 gauss field,  $\rho = 480$  cm. Thus, for a path length  $X = 10$  cm,  $Y = 0.1$  cm. Y decreases as electron energy increases.

The earth's magnetic field (~0.5 gauss) does not present a problem as long as the collector diameter

is greater than 0.2X. However, one must exercise due care in the vicinity of larger fields.

- 4.) Rutherford backscattering of incident electrons out of the collector.

The cross section for non-relativistic Rutherford backscattering from target nuclei is given by Evans (Ref. 5)

$$\sigma(\theta > \frac{\pi}{2}) \cong \frac{1}{4} \frac{Z^2}{\beta^4} \text{ where } \beta = \frac{\text{electron velocity}}{\text{velocity of light}}$$

Then, the fraction,  $\eta$ , of incident electrons backscattered from a thin foil of element (Z,A), density  $\rho$ , and thickness  $dS$  is given by

$$\eta = \sigma(\theta > \frac{\pi}{2}) \cdot \frac{N_0}{A} \cdot \rho dS$$

For a thick target, let us assume that  $\rho dS$  equals  $R_0$ , the range of an electron in the material.

Then, for a 10 keV electron energy in Al,  $R_0 = \rho dS = 0.2 \frac{\text{mg}}{\text{cm}^2}$  (Ref. 5, pg. 624).

Thus, for aluminum

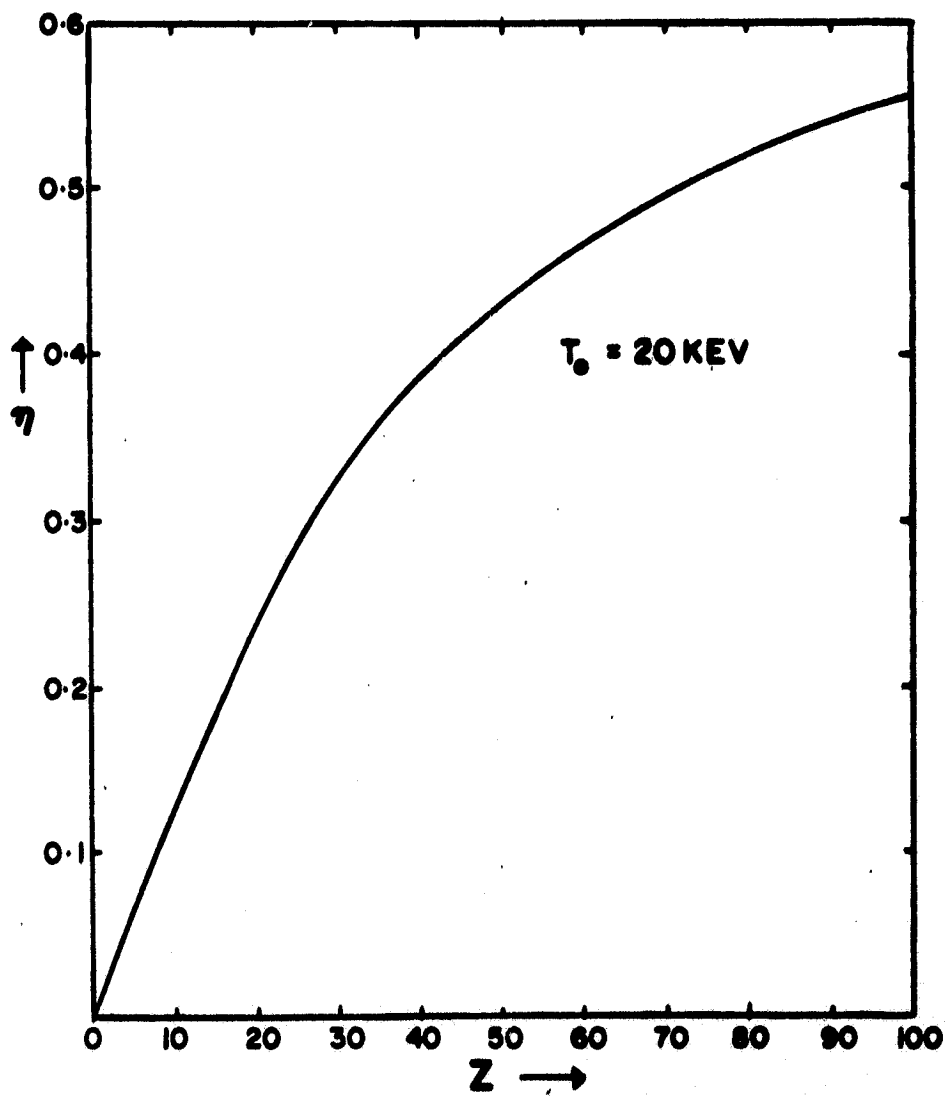
$$\eta \cong \frac{Z^2}{4\beta^4} \cdot \frac{N_0}{A} \cdot \rho dS \cong 12\%$$

For carbon, this will be down to about 3%. Contrast this to the measured backscatter data presented by Duscumb and Reed (Ref. 9). (See Figure

4-1.) For carbon  $\eta = 7\%$  and for Al,  $\eta = 16\%$ . But the energy distribution of electrons backscattered from light nuclei in a thick target, peaks at about  $\frac{1}{2} T_0$ , where  $T_0$  is the incident electron energy. As far as X-ray producing capabilities are concerned, our crude model is remarkably accurate. We can also see the advantage in lining the collector with a light element like carbon. If the collector length is 10 times its diameter, the solid angle for escape is  $\sim 10^{-2}$  steradians, and  $\eta \frac{\Omega}{2\pi} \approx 4 \times 10^{-5}$  for carbon. The geometry should be such that none of these escaping electrons strike the chamber wall within the detector field of view. We can always add some baffles to the collector interior to reduce  $\Omega$ , the solid angle of escape. Auger electron production in the collector also represents a potential source of background. This is true especially for low Z materials where fluorescence yields of less than 1% are encountered. We can estimate  $\eta_A$ , the number of Auger electrons produced per incident primary electron by

$$\eta_A \approx Q \cdot \frac{N_0}{A} \cdot \rho dS$$

where  $Q =$  the k-shell ionization cross section.



FRACTION OF ELECTRONS BACKSCATTERED (WITH INCIDENT BEAM NORMAL TO SURFACE) AS A FUNCTION OF TARGET ATOMIC NUMBER

FIG. 4-1

Using the equations presented in Section 6.0, we calculate that  $Q \approx 1 \times 10^{-26} \text{ cm}^2$  for 10 kev electrons on Al. Again, assuming  $\rho dS = R_0$ , the range of a 10 kev electron in aluminum, we deduce

$$\eta_A \approx 10^{-26} \cdot \frac{6 \times 10^{23}}{27} \cdot 2 \times 10^{-4} = 4.4 \times 10^{-8}$$

a completely negligible quantity.

In addition to backscattered electrons, the collector serves as a copious source of thick target bremsstrahlung. We can get a feeling for the intensity in the following way.

From Evans (Ref. 5, pg. 617), we find that the fraction of the electron energy converted into bremsstrahlung from a thick target equals  $7 \cdot EZ \times 10^{-7}$ . We may also write this fraction as the ratio of X-ray intensity to electron energy,  $\frac{I}{E}$ . Thus we arrive at

$$\frac{I}{E} = 7 \cdot EZ \times 10^{-7}.$$

For 5 kev electrons incident on a carbon target

$$\frac{I}{E} = 2.1 \times 10^{-5}$$

Now, a 1 mA beam corresponds to  $6.25 \times 10^{15}$  electrons per second. Hence, the total bremsstrahlung energy is

$$I = 6.25 \times 10^{15} \times 2.1 \times 10^{-5} \times 5 \frac{\text{kev}}{\text{sec}} = 6.57 \times 10^{11} \frac{\text{kev}}{\text{sec}}$$

Let us assume that all the X-rays have the same energy,  $E$ , equal to the energy at the thick target spectral peak, i.e.  $E = \frac{2}{3} T_0 = 3.3 \text{ kev}$ .

Then, the number of thick target X-rays produced per second is  $n = 2 \times 10^{11} \frac{\text{photons}}{\text{sec}}$  into  $2\pi$ . If the solid angle of the collector cup is  $10^{-2}$  steradians, then the number of X-rays per second escaping into the chamber is  $2 \times 10^8$  per second. Assume that all of these photons strike the chamber wall within the detector field of view. We then estimate the number which are scattered into the detector. At the low energies being considered, the predominant mechanism is classical Thompson scattering. The Thompson cross section is given by

$$\sigma_0 = 0.665 \times 10^{-24} \frac{\text{cm}^2}{\text{electron}} .$$

If the chamber walls are coated with carbon ( $Z = 6$ ), then the cross section per atom is  $6\sigma_0$  or  $4 \times 10^{-24} \frac{\text{cm}^2}{\text{atom}}$ . The fraction of incident X-rays scattered into  $2\pi$  steradians is

$$F = \frac{\Delta n}{n} = \frac{Z\sigma_0}{2} \frac{N_0}{A} \cdot \rho_w t_w$$

$\rho_w t_w$  = The "effective" thickness of the chamber wall. We assume this equal to one absorption length of a 3.3 keV X-ray in the material. For carbon, this equals 18.13 mg/cm<sup>2</sup>.

Then  $F = \frac{4.0 \times 6 \times 10^{23} \times 0.0181 \times 10^{-24}}{2 \times 12} = 1.8 \times 10^{-3}$  and  $\Delta n = 3.6 \times 10^5 \frac{\text{photons}}{\text{sec}}$  are Thompson scattered from the wall. If the detector subtends a solid angle of  $10^{-3}$  steradians, scattered photons will reach the detector face at a rate of

36 per second. Recall that this is if all collector produced X-rays strike the chamber wall in the detector field of view. Again we arrive at the conclusion that detector and collector fields of view should not intersect at the chamber wall.

Finally, we considered Thompson scattering of collector produced X-rays from gas molecules within the detector field of view. The ratio of Thompson scattered collector X-ray flux to bremsstrahlung yield within the detector field of view is at most 0.01%.

The following statements summarize the results of the above analysis and represent a set of design guidelines.

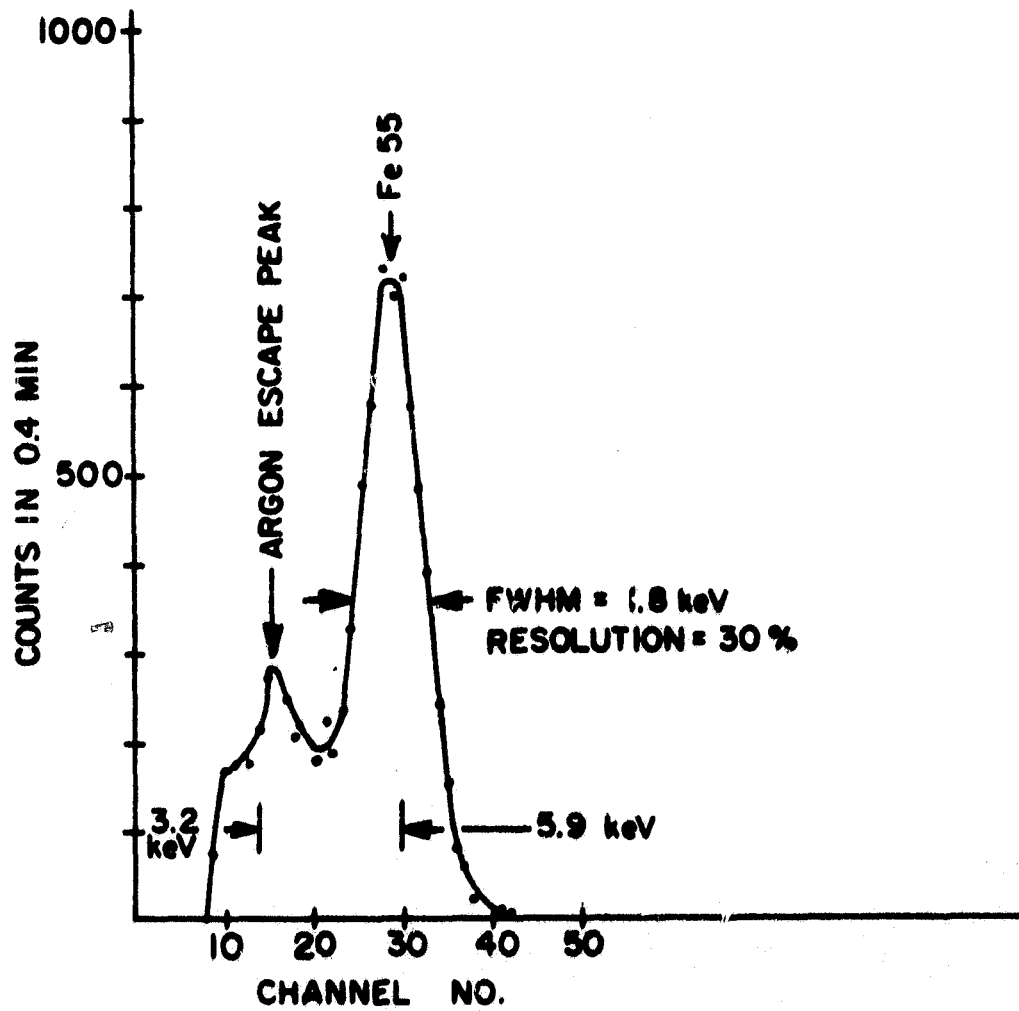
- 1.) The detector field of view and the collector field of view (as seen from the rear of the collector) must not intersect at the chamber wall.
- 2.) Line the chamber and collector with a low Z material to reduce electron backscattering and spurious bremsstrahlung production.
- 3.) The collector field of view must be as small as possible.
- 4.) Produce a narrow, well defined beam with the electron gun.
- 5.) Use care in the presence of moderate magnetic fields.

## 5.0 EXPERIMENTAL RESULTS

Most experimental programs suffer from delays, unforeseen difficulties and equipment breakdowns; this one was no exception. In spite of this, we were able to take sufficient data to demonstrate the feasibility of constructing a vacuum gauge in a small chamber.

Figure 5-1 shows the energy calibration of the multi-channel analyzer and proportional counter. Operating conditions for this experiment appear in Table III. The source consisted of an 80  $\mu\text{Ci}$   $\text{Fe}^{55}$  source (5.9 keV X-rays). In addition, we found no spurious background counts when the source was placed in the chamber at high vacuum, but out of the detector field of view (Refer to Figure 5-2). We present a typical measured bremsstrahlung spectrum in Figure 5-3, which should be compared with the spectrum predicted by the computer program and shown in Figure 5-4.

The discrepancy in shape between the experimental spectrum and the predicted spectrum results from the argon fill gas. Approximately 10% of the photons entering the counter deposit 3.2 keV less than their full energy as argon fluorescent X-rays escape. Figure 5-5 shows a calculated spectrum, corrected for the argon escape peak. This distribution matches the general features, such as relative peak heights, better than the uncorrected version. Counter reso-

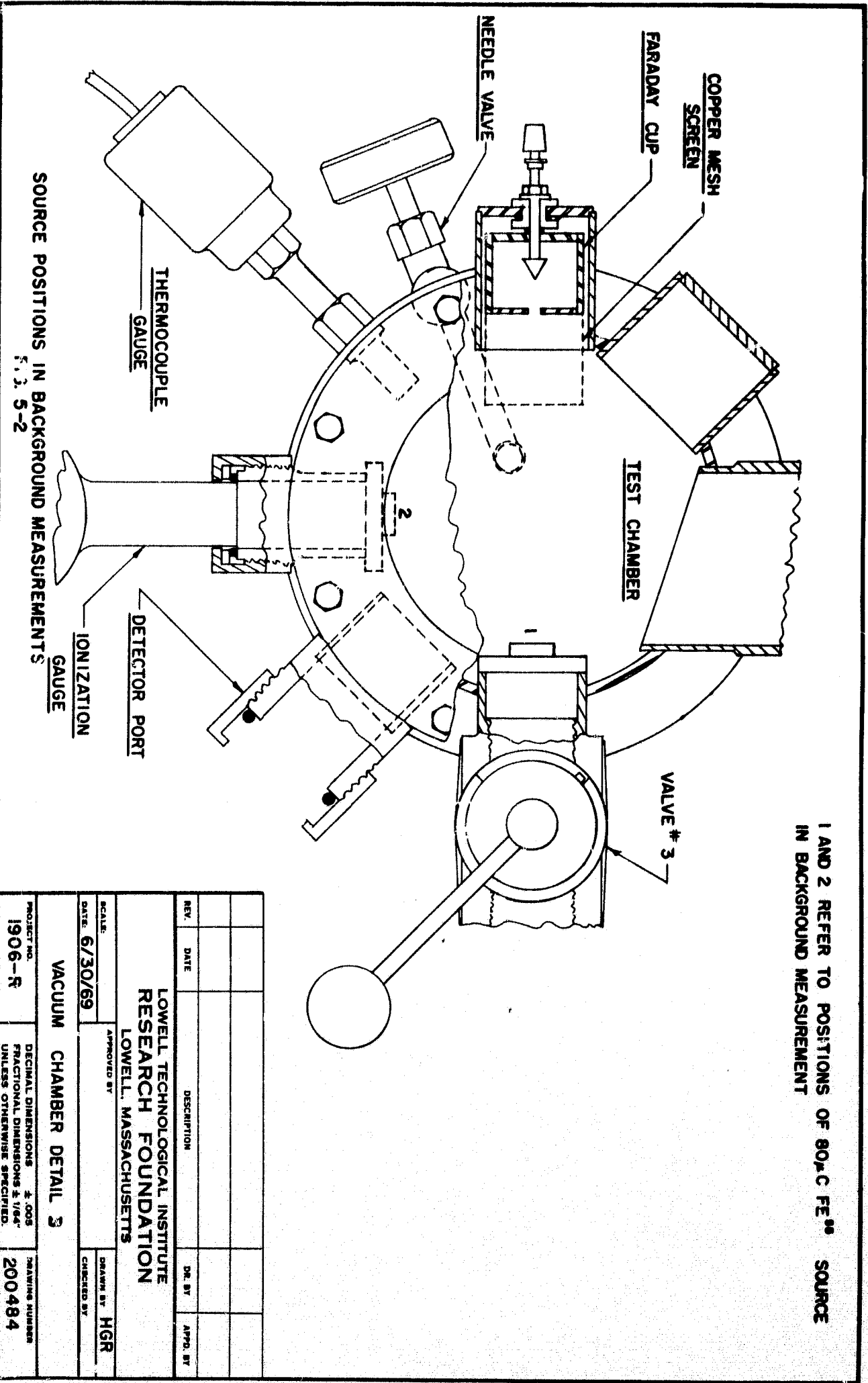


$Fe^{55}$  CALIBRATION SPECTRUM  
FIG. 5-1

TABLE III

EXPERIMENTAL CONDITIONS

Equipment:	TMC Gammascoppe II Model 102
Settings:	Expansion        X1
	Threshold        5
	Gain             1000
	Upper Level     10
	Baseline         0
Pulse Height Analysis:	Use .4 min. live time
Multiscale:	Use 1 sec. dwell time, 0 threshold, 490 window
HV = 1490V	Counter = 310 PC with Ar and CH <sub>4</sub>
Calibration Source:	5.9 kev X-rays from 80 $\mu$ Ci Fe <sup>55</sup> source



1 AND 2 REFER TO POSITIONS OF 80 $\mu$ C FE<sup>99</sup> SOURCE IN BACKGROUND MEASUREMENT

SOURCE POSITIONS IN BACKGROUND MEASUREMENTS

FIG. 5-2

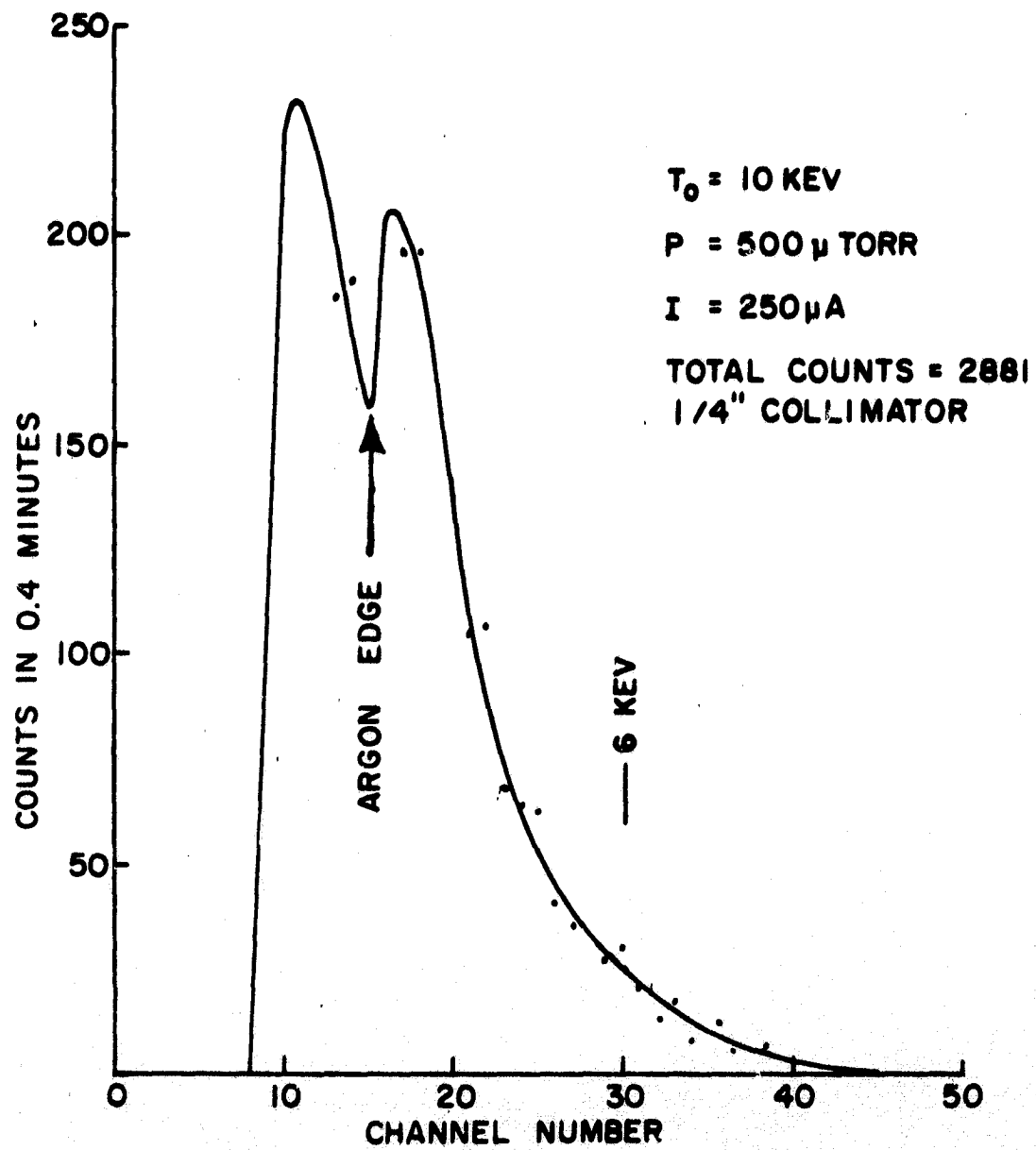
REV.	DATE	DESCRIPTION	DR. BY	APPR. BY

SCALE:   
 DATE: 6/30/69   
 APPROVED BY:   
 DRAWN BY: HGR   
 CHECKED BY:

LOWELL TECHNOLOGICAL INSTITUTE   
 RESEARCH FOUNDATION   
 LOWELL, MASSACHUSETTS

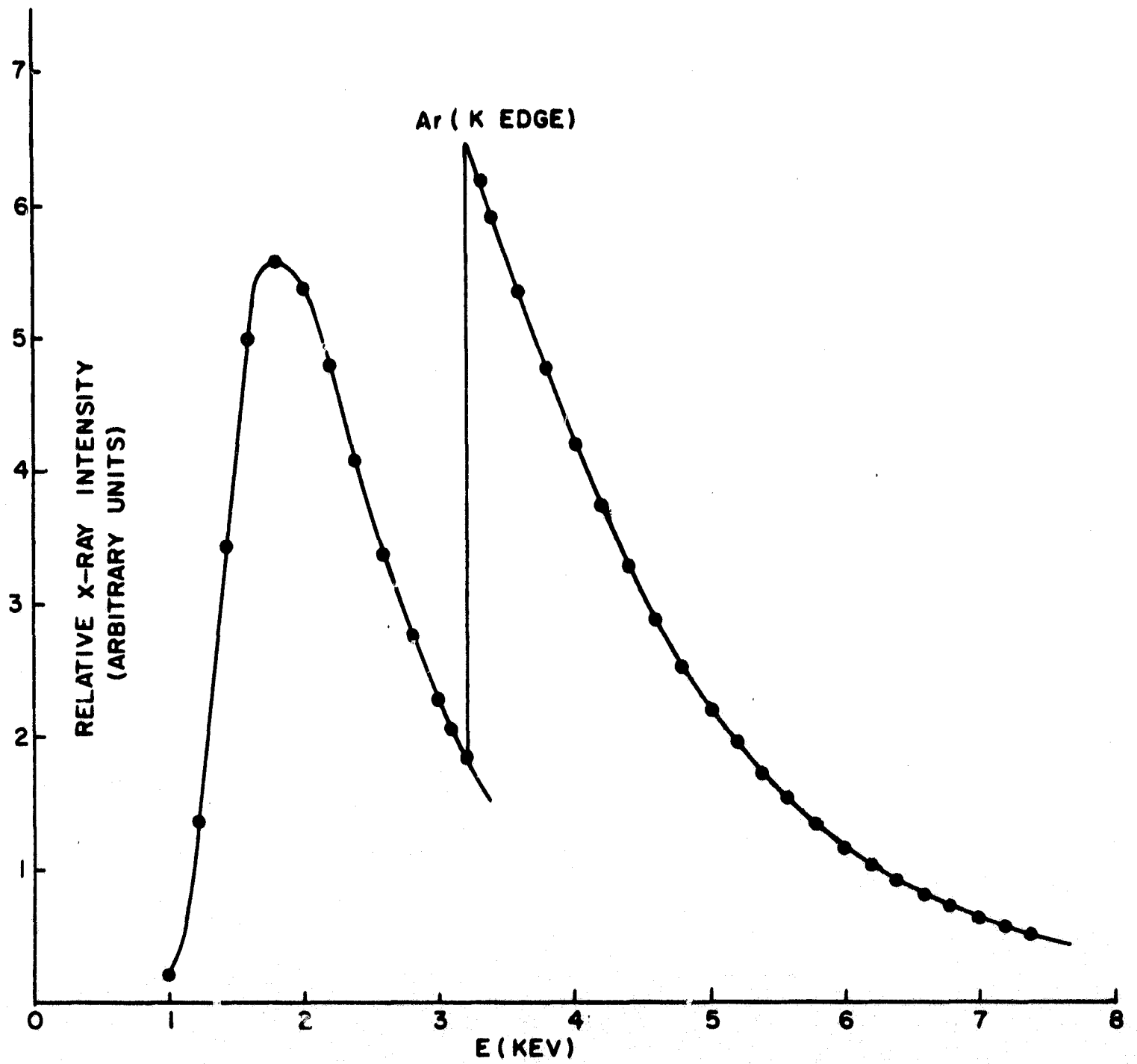
VACUUM CHAMBER DETAIL 3

PROJECT NO. 1906-R	DECIMAL DIMENSIONS ± .005 FRACTIONAL DIMENSIONS ± 1/64" UNLESS OTHERWISE SPECIFIED.	DRAWING NUMBER 200484
--------------------	---	-----------------------



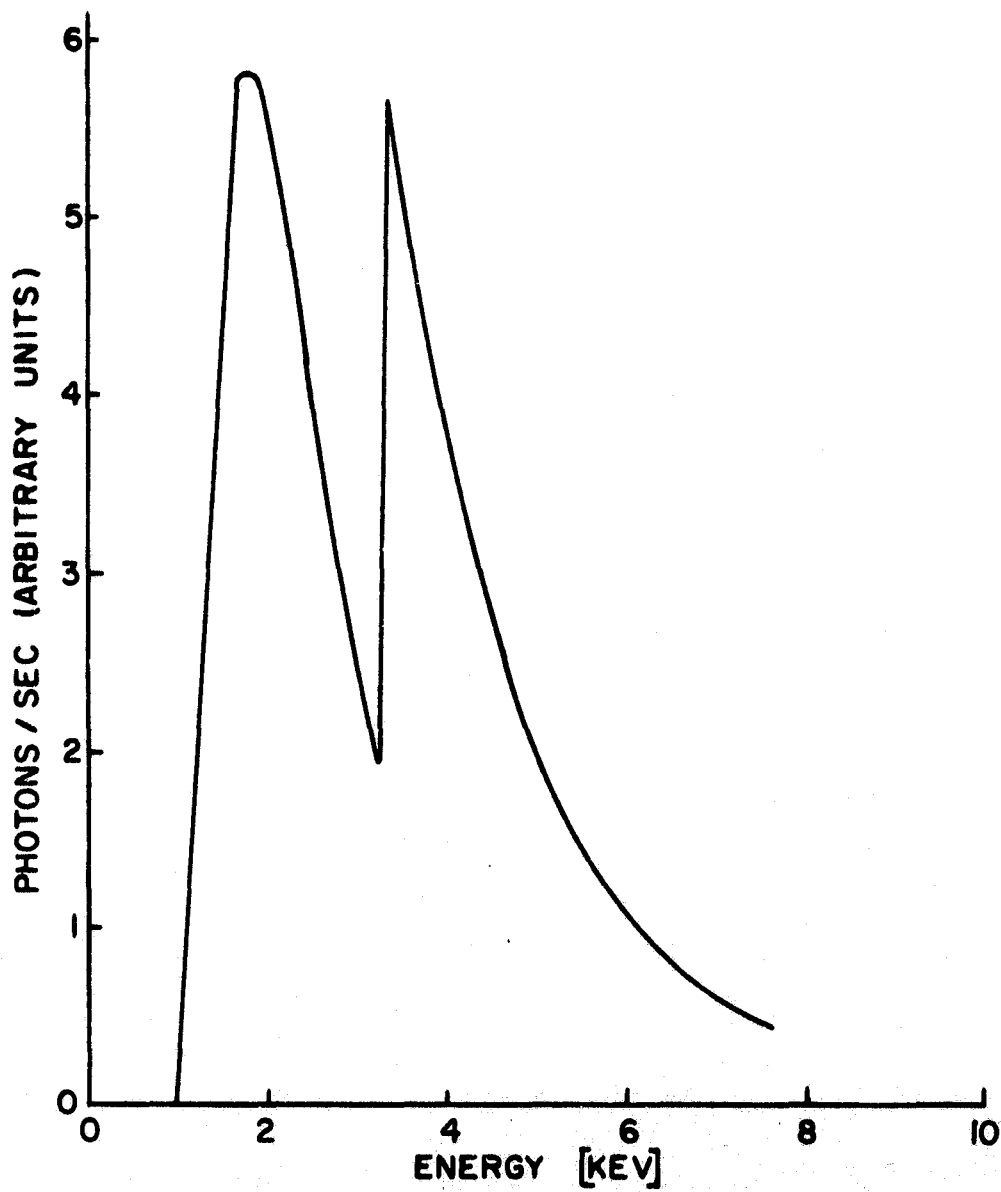
TYPICAL MEASURED  
BREHMSSTRAHLUNG SPECTRUM

FIG. 5-3



COMPUTED SPECTRUM FOR AIR AT  $T_0 = 10\text{KEV}$   
(P-10 COUNTER FILL)

FIG. 5-4



COMPUTED SPECTRUM FOR AIR  
AT  $T_0 = 10$  KEV, CORRECTED FOR ESCAPE  
PEAK OF ARGON IN P-10 FILL

FIG. 5-5

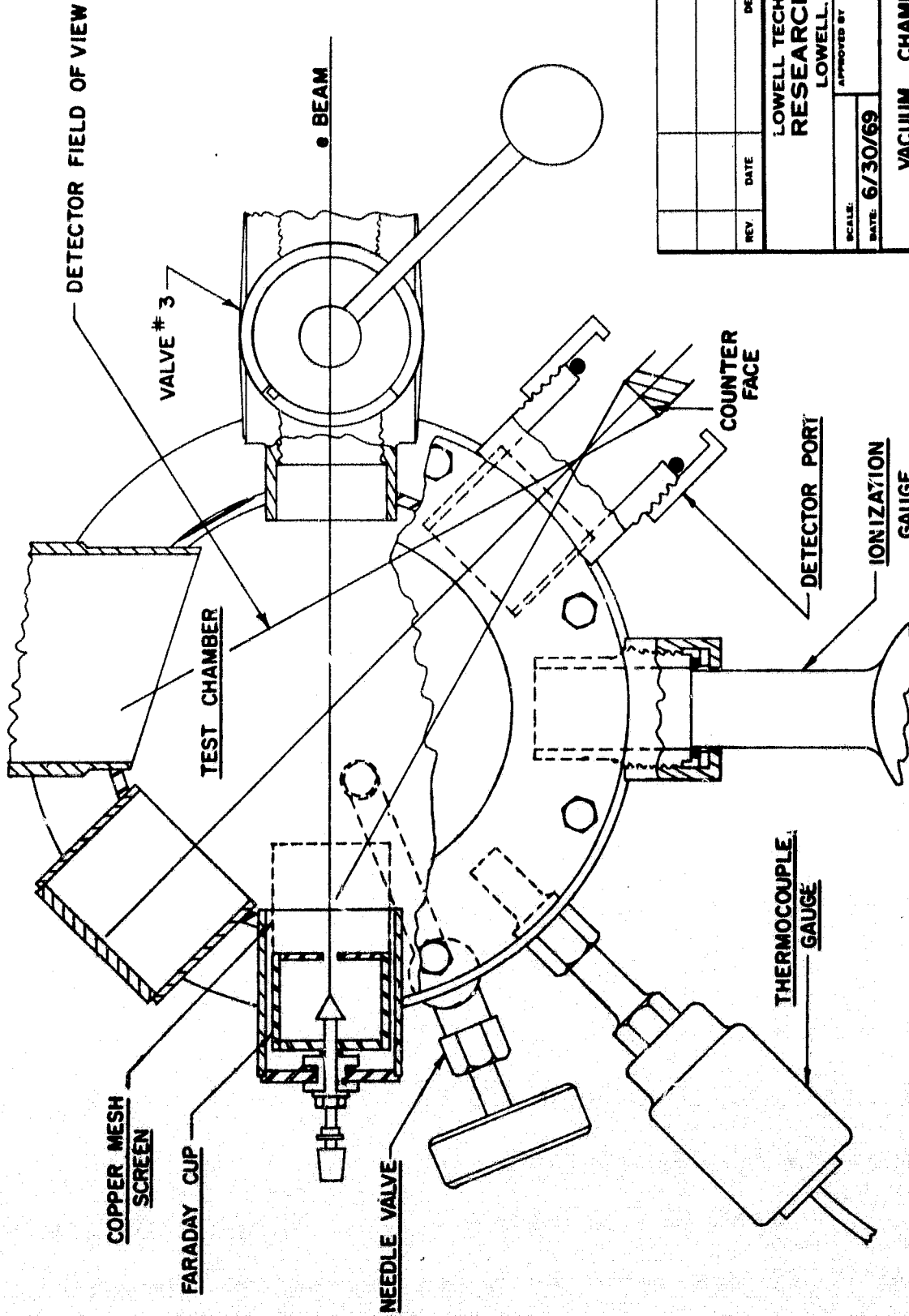
lution tends to fill in the absorption edge in the measured curve.

Previous work, performed in a larger chamber at Langley Research Center, demonstrated linearity of response and, ultimately, low backgrounds (Ref. 10). Our problem here centered on producing results in a chamber only 4 inches in diameter and 2 inches long.

In such a small chamber, X-rays generated by electrons striking the Faraday cup constitute the largest source of pressure-independent counts. Natural background radiation gives a lower bound to the achievable reduction and limits the ultimate sensitivity of the gauge as discussed elsewhere in this report.

The electron beam entered the chamber at an angle, apparently because of deflections by the earth's magnetic field. Because of this, a small magnet was necessary to deflect the beam into the Faraday cup. All data presented hereafter assumes the use of such a magnet unless otherwise specified.

Initially we removed the collimator from the detector (See Figure 5-9) and we also removed the screen and aperture plate of the Faraday cup. We could not otherwise position the beam inside the Faraday cup reliably. We used a magnet at the collector, adjusted to minimize the count



EXPERIMENTAL GEOMETRY WITH NO COLLIMATOR  
FIG. 5-3

REV.	DATE	DESCRIPTION	DR. BY	APPR. BY

LOWELL TECHNOLOGICAL INSTITUTE  
RESEARCH FOUNDATION  
LOWELL, MASSACHUSETTS

APPROVED BY: MGR  
DRAWN BY: MGR  
CHECKED BY: MGR

SCALE: 6/30/69  
DATE: 6/30/69

VACUUM CHAMBER DETAIL D

PROJECT NO. 1906-R  
DECIMAL DIMENSIONS & .008  
FRACTIONAL DIMENSIONS & 1/64"  
UNLESS OTHERWISE SPECIFIED.

DRAWING NUMBER 200493

rate at a low pressure. All surfaces except the top plate were carbon coated to reduce X-ray production and electron backscatter.

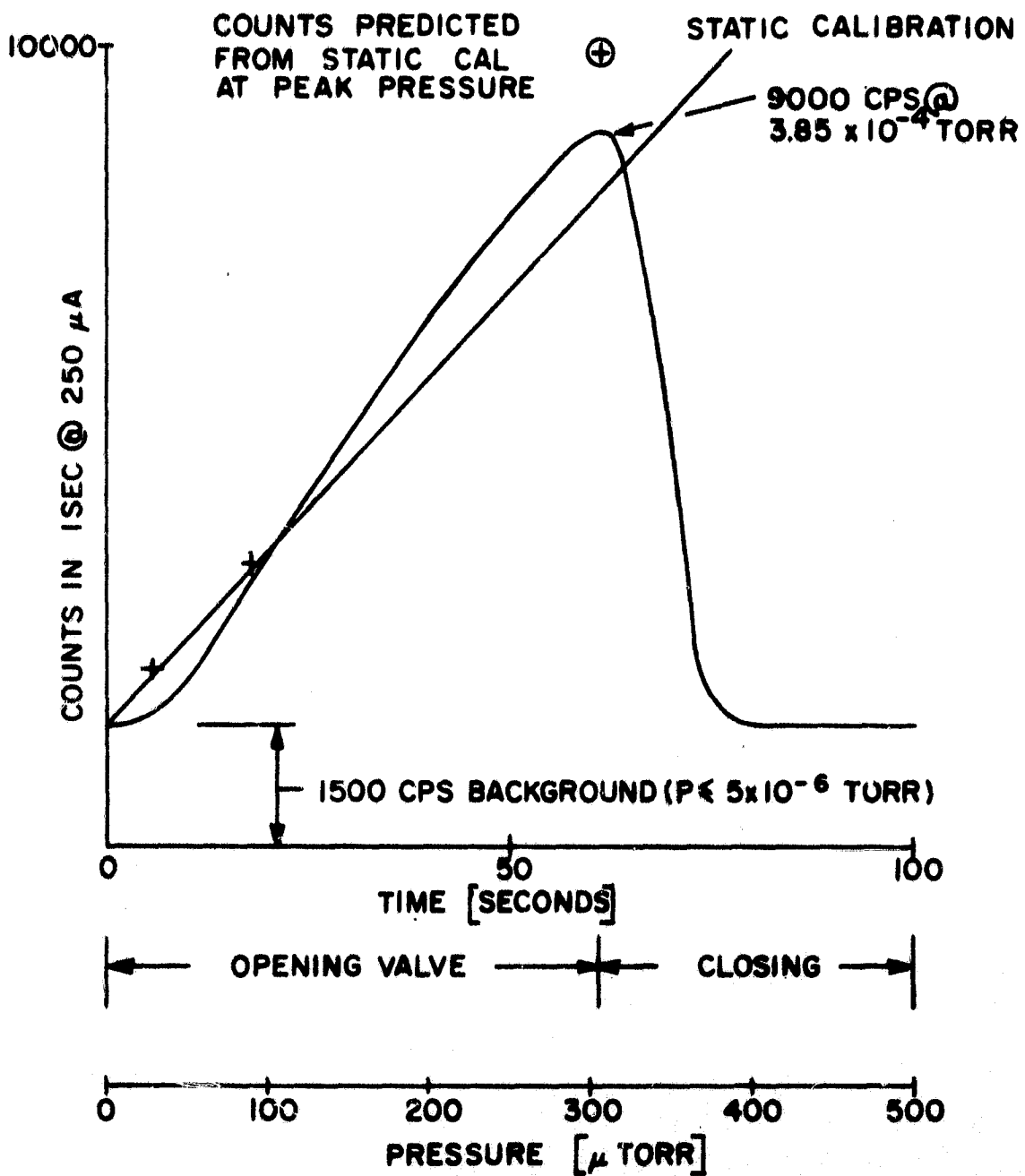
Then we varied the pressure, as read from the ion gauge, and recorded the number of X-rays detected each second. We took three points at 90, 30, and  $3\mu\text{Torr}$ , from which a least squares fit gave 6091 cps/mA independent of pressure and 87.14 cps/MA/ $\mu\text{Torr}$  as a slope. This data comprises the static calibration plotted in Figure 5-6.

Using the multiscaling feature of the pulse-height analyzer, we proceeded to take a series of 100 one-second counts as we raised the pressure to 385  $\mu\text{Torr}$ , then decreased it. We plotted this data in Figure 5-6, Dynamic Response of Gauge.

From this data we see that one-second measuring times can yield significant signal to noise ratios. Also, the time scale indicates a smooth gauge response. At the highest pressure, the observed dynamic count rate differs from the expected value by only 10%. That may result from calibration uncertainty rather than a true dynamic response.

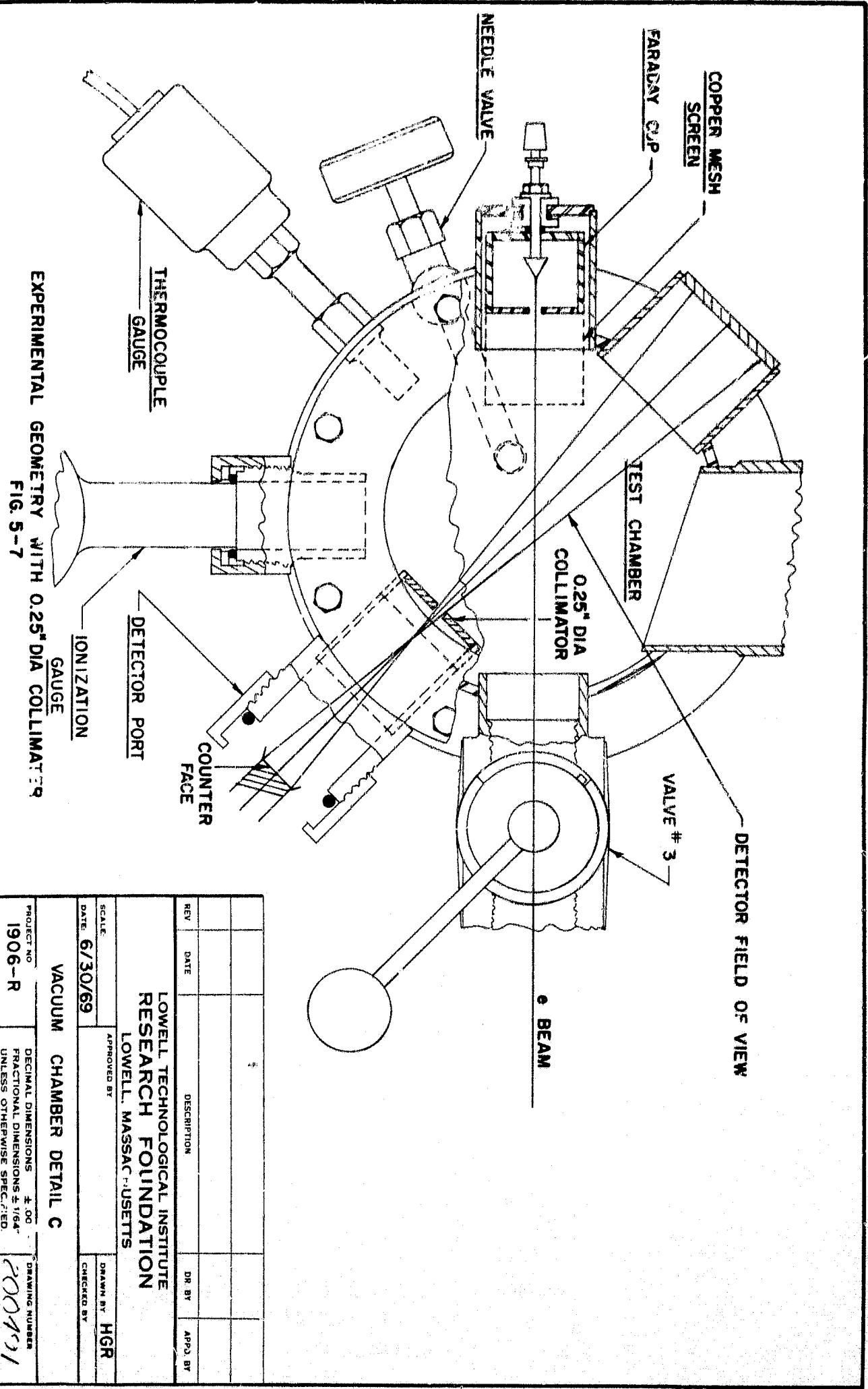
In any event, this curve clearly shows the practicality of our gauge in a small chamber. Even minimal precautions against background result in a gauge usable over two orders of magnitude.

Next we installed a  $1/4$ " diameter collimator as shown in Figure 5-7. We again varied the pressure, over the



DYNAMIC RESPONSE OF GAUGE  
(NO COLLIMATOR)

FIG. 5-6



EXPERIMENTAL GEOMETRY WITH 0.25" DIA COLLIMATOR  
 FIG. 5-7

REV	DATE	DESCRIPTION	DR. BY	APP. BY

SCALE: \_\_\_\_\_  
 DATE: 6/30/69  
 APPROVED BY: \_\_\_\_\_  
 DRAWN BY: HGR  
 CHECKED BY: \_\_\_\_\_

VACUUM CHAMBER DETAIL C  
 LOWELL TECHNOLOGICAL INSTITUTE  
 RESEARCH FOUNDATION  
 LOWELL, MASSACHUSETTS

PROJECT NO: 1906-R  
 DECIMAL DIMENSIONS ± .00  
 FRACTIONAL DIMENSIONS ± 1/64"  
 UNLESS OTHERWISE SPECIFIED

DRAWING NUMBER: 200491

range from 4  $\mu$ Torr to 500  $\mu$ Torr as indicated by the ionization gauge. The ion gauge controller does not regulate the emission current to exactly 1.0 mA on the 1000  $\mu$ Torr (full scale) range; we corrected the reading by a factor of 1/1.3 to account for this discrepancy.

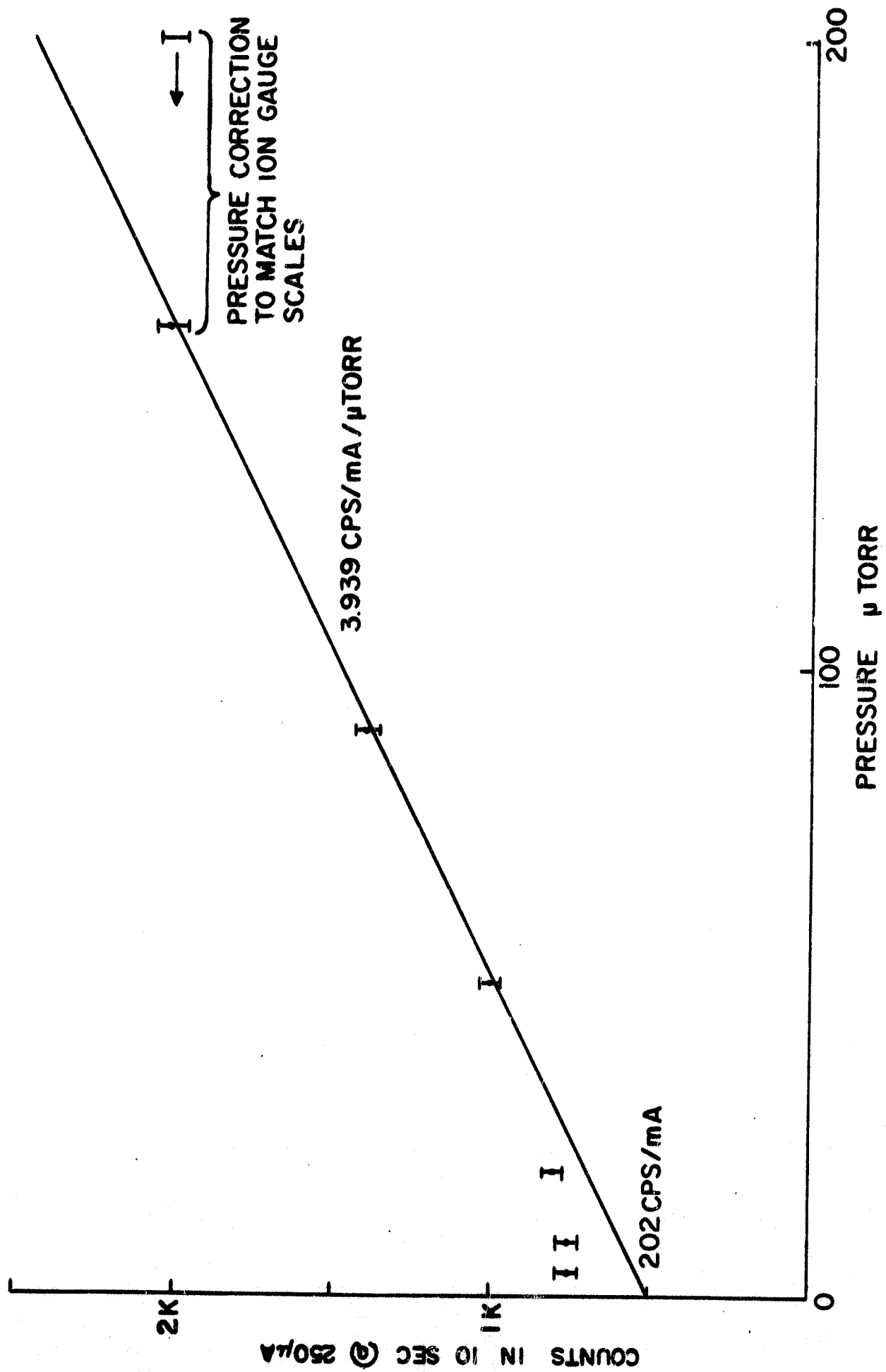
We measured this correction factor by setting the system pressure to 100  $\mu$ Torr as measured on the 100  $\mu$ Torr (full scale) range, then reading the gauge on the 1000  $\mu$ Torr scale; since the gauge then indicated 130  $\mu$ Torr, we must divide all readings on the highest scale by 1.3.

Figure 5-9 shows the curve that results from making a least squares fit to the three highest points only. All data points show error bars corresponding to expected one-sigma statistical variations of the number of observed X-rays. The obvious flattening of the curve at low pressure justifies excluding them from the curve fitting; the resulting estimate of the pressure independent intercept lies below the observed values. We did not include the highest pressure point in the analysis because the beam current was unstable.

Although the measured response per unit pressure should have produced changes of count rate below 10  $\mu$ Torr, the observed count rates were constant. Also, the experimental data at low pressures exceeds the background derived by extrapolating the slope to zero pressure. This requires that we postulate another response which decreases with increasing

+

+



MEASURED RESPONSE USING 0.25" DIAMETER COLLIMATOR

FIG. 5-9

+

+

pressure. X-ray attenuation at these pressures cannot provide the 50% reduction necessary to account for the observed change, so we must look for another mechanism.

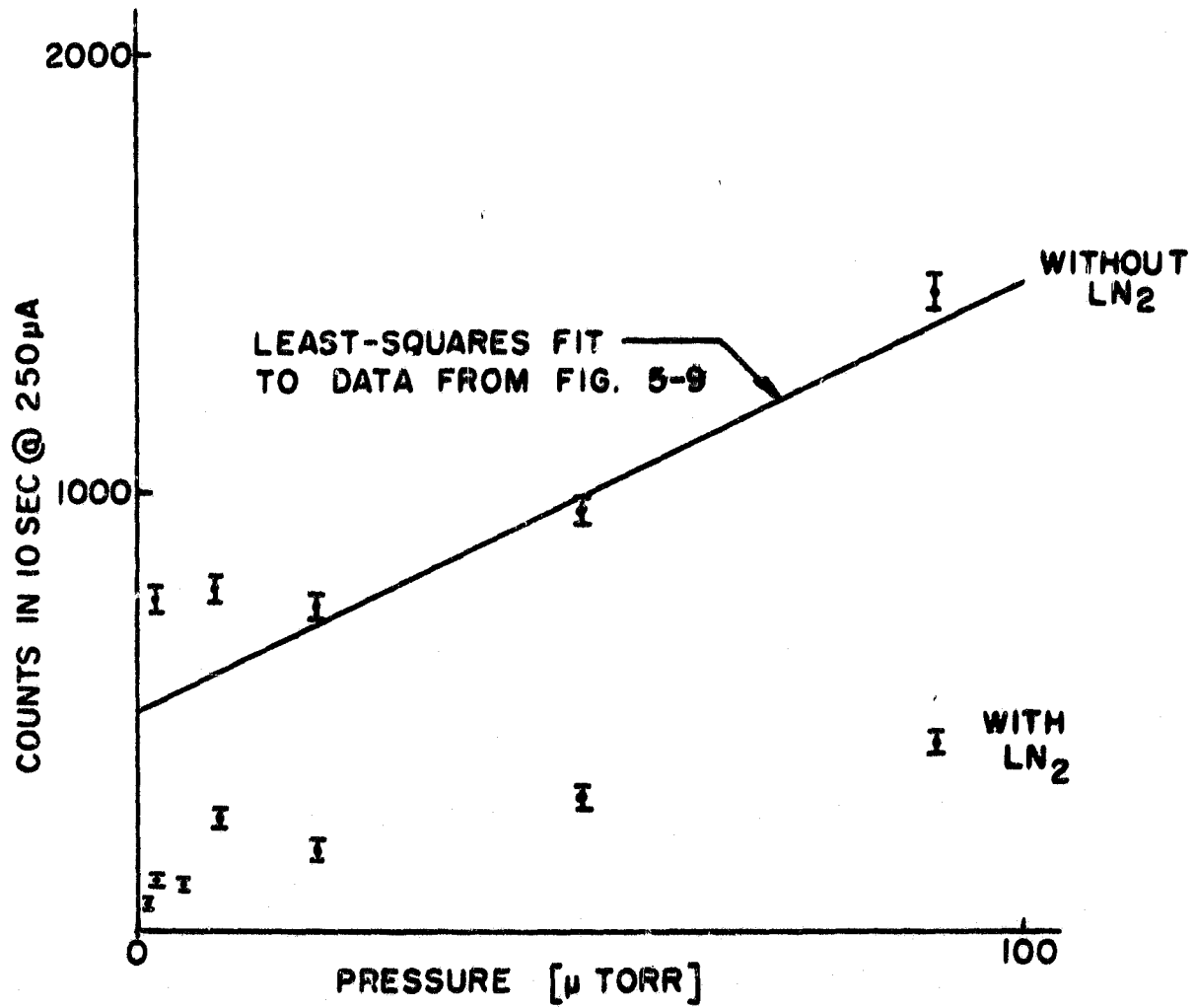
We felt that the higher response at low pressures resulted from either a change of composition or a pressure induced variation of beam position. To differentiate between these alternatives, we made another pair of tests.

First, we repeated the experiment as run before. Second, we filled the reservoir with liquid nitrogen, hoping that composition changes would be revealed.

Prior to repeating the experiment, we had to reposition the collector magnet to minimize the X-ray background. In addition the proportional counter bias was accidentally set to 1480 volts rather than 1490. In spite of these variations, the measured values fall close to the original curve as seen in Figure 5-10.

When we added liquid nitrogen to the trap, the count rates fell dramatically at the lowest pressures. As we varied the pressure, we observed increasing count rates. These points appear in Figure 5-10 well below the points taken without cooling the system.

This last data presents some puzzling questions. Even by eye, we see that the response per unit pressure decreased with cooling. Since the readings correspond to equal pressures on the ionization gauge, between 50 and 90  $\mu$ Torr



MEASURED RESPONSE WITH AND WITHOUT LIQUID NITROGEN (0.25" DIAMETER COLLIMATOR)

FIG. 5-10

we expect the same slope. In each case, we admitted room air to generate pressures at least ten times the baseline pressure. Composition should have remained constant, thus yielding equal slopes. This portion of the data argues for a change of beam position, perhaps induced by the temperature difference between gun chamber and test chamber. Such a change in relative position could also reduce the X-ray background.

An alternative effect results from the increase of differential pressure between the gun and test chambers. Since we adjusted the beam current to 250  $\mu$ A for each condition, the cathode current variation with pressure could have been different. Using nitrogen cooling would tend to create less poisoning of the cathode as the pressure is increased. This would provide a more constant load for the unregulated power supply that sets the beam energy. A quick test revealed that small (1.0%) changes of beam energy varied the background count rate by at least one order of magnitude.

This strong relation of the background X-ray production to the beam energy results from the magnetic deflections of the beam. First, the earth's magnetic field acts on the beam to give it an initial deflection. Secondly, we minimize the background by sharply deflecting the beam, at the collector, with a strong magnet. Experimentally, we observe a very sharp minimum as the magnet position changes, as well as a sharp minimum when the voltage varies.

In terms of the ratio of gas-induced counts to background, the data at the lower part of Figure 5-10 may represent a factor of two reduction of the pressure at which the gas-induced counts equal the background counts.

Thus, in spite of the limitations of our experimental apparatus and the brief time available, we are very encouraged to find reasonable signal-to-noise ratios at pressures as low as 50  $\mu$ Torr.

Additional effort, of the kind outlined elsewhere in this report, will further reduce the background and may simultaneously increase the slope, permitting extensions to lower pressures.

## 6.0 THE POSSIBILITY OF USING CHARACTERISTIC X-RAYS TO DETERMINE GAS COMPOSITION

If the electron beam energy is greater than the k ionization potential of the target gas, characteristic k X-rays are produced; discrete lines are superimposed on the bremsstrahlung continuum. By measuring the intensity of these k lines, we can determine the atomic composition of the gas under investigation.

The feasibility of this technique clearly depends on the ratio of k X-ray flux to bremsstrahlung flux reaching the detector. Our analysis considers the situation in which characteristic X-rays produced in  $\text{CO}_2$  are detected by a proportional counter having a spectrally selective window to filter out much of the bremsstrahlung background.

### 6.1 Carbon K Radiation ( $44\overset{\circ}{\text{A}}$ )

We considered the intensity of carbon k radiation at  $44\overset{\circ}{\text{A}}$  (282 ev) produced by 500 volt electrons. This low energy was chosen to enhance the k shell ionization cross section and to inhibit the bremsstrahlung yield at higher energies. An expression for the ionization cross section was first derived by Bethe (Ref. 11) in 1930; we used the treatment by Worthington and Tomlin (Ref. 12) as a basis for our calculation. The appropriate formula is

$$Q V_k^2 = 0.7 \pi e^2 \frac{1}{U} \ln \frac{4U}{B}$$

where  $Q$  is the ionization cross section, i.e. the number of ionizations per atom per incident electron per  $\text{cm}^2$ .

$V_k$  = ionization potential of the  $k$  shell, i.e. 282 ev for carbon.

$e$  = electronic charge =  $4.8 \times 10^{-10}$  esu

$V$  = electron accelerating potential = 500 volts in this case.

$$U = \frac{V}{V_k} = 1.77$$

$$B = [1.65 + 2.35 \exp(1-U)] = 2.737$$

We performed the calculation and arrived at

$$Q = 3.425 \times 10^{-24} \text{ cm}^2.$$

Not all of the  $k$  shell ionizations result in X-rays; we must consider the competition with Auger electron production. Indeed for light elements, Auger production is the prime mode of de-excitation. The fluorescence yield is defined as the number of  $k$  X-rays produced per  $k$  shell vacancy, and varies approximately as  $Z^4$  for light elements (Ref. 13). We were unable to find a value of the carbon fluorescence yield in the literature and we therefore extrapolated from the theoretical value for oxygen, i.e. 0.0045. In this way we obtained a value of 0.0014 for carbon. Multiplying  $Q$  by the fluorescence yield produces  $\sigma_k = 5.32 \times 10^{-27} \text{ cm}^2$ , the cross section for characteristic X-ray production.

Let us now consider a counter having a polypropylene (CH<sub>2</sub>) window. The counter efficiency,  $\epsilon(E)$  is given by the window transmission coefficient, since at the low energies being considered, the counter gas may be considered opaque. We calculated the counter efficiency as a function of energy using the experimental data of Henke et al (Ref. 14). Figure 6-1 illustrates the results.

On the same figure we plot the differential cross section for bremsstrahlung production from CO<sub>2</sub>. The cross section per molecule is given by

$$\left. \frac{d\sigma}{dE} \right|_{\text{CO}_2} = \left. \frac{d\sigma}{dE} \right|_{\text{C}} + 2 \left. \frac{d\sigma}{dE} \right|_{\text{O}}$$

For simplicity, we used the non-relativistic formula given in Evans (Ref. 5).

$$\frac{d\sigma}{dE} = \frac{16}{3} \sigma_0 Z^2 \frac{1}{E}$$

where E is the photon energy.

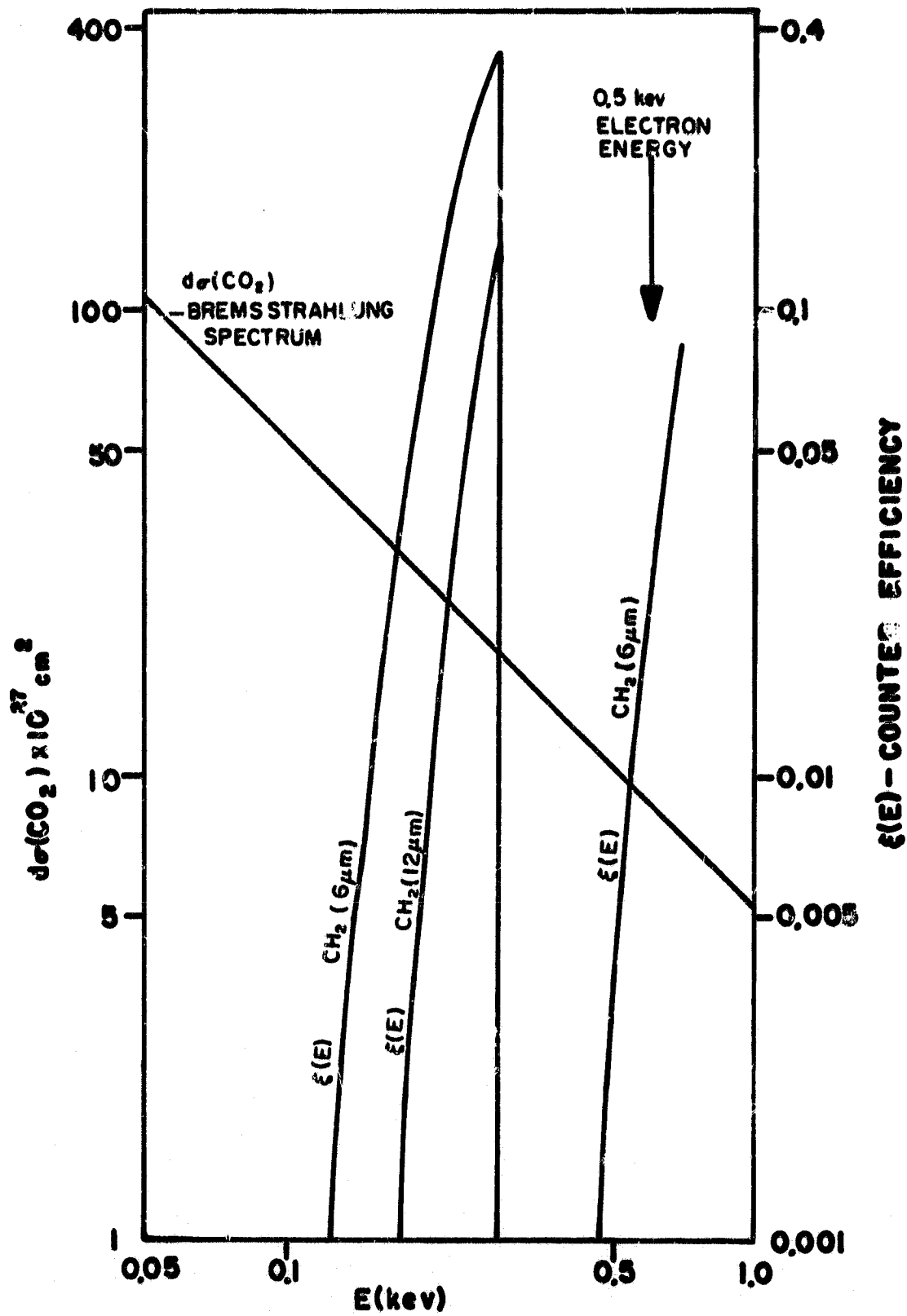
Z is the atomic number of the target nucleus.

$$\sigma_0 = 0.58 \times 10^{-27} \text{ cm}^2$$

Then for CO<sub>2</sub>, and dE = 0.01 kev

$$d\sigma = \frac{5.07 \times 10^{-27} \text{ cm}^2}{E \text{ (kev)}}$$

We then calculated the number of photons detected per molecule per electron per cm<sup>2</sup>, i.e. the integral  $\int \epsilon(E) d\sigma(E)$  was evaluated graphically. (Figure 6-1.)



COUNTER EFFICIENCY VS. ENERGY  
(POLYPROPYLENE WINDOW)

FIG. 6-1

696001

For a 12  $\mu\text{m}$  window,  $\int \epsilon(E) d\sigma(E) = 8.31 \times 10^{-26} \text{ cm}^2$ . This must be compared to  $\sigma_k \cdot \epsilon(282 \text{ ev})$ , i.e. the signal to noise ratio is given by

$$\left(\frac{S}{N}\right)_{12 \mu\text{m}} = \frac{\sigma_k \cdot \epsilon(282 \text{ ev})}{\int_{12 \mu\text{m}} \epsilon(E) d\sigma} = 7.75 \times 10^{-2}$$

For a 6  $\mu\text{m}$  window,  $\int \epsilon(E) d\sigma_B(E) = 27.4 \times 10^{-26}$ . Then,

$$\left(\frac{S}{N}\right)_{6 \mu\text{m}} = \frac{\sigma_k \cdot \epsilon(282 \text{ ev})}{\int_{6 \mu\text{m}} \epsilon(E) d\sigma_B} = 6.78 \times 10^{-2}$$

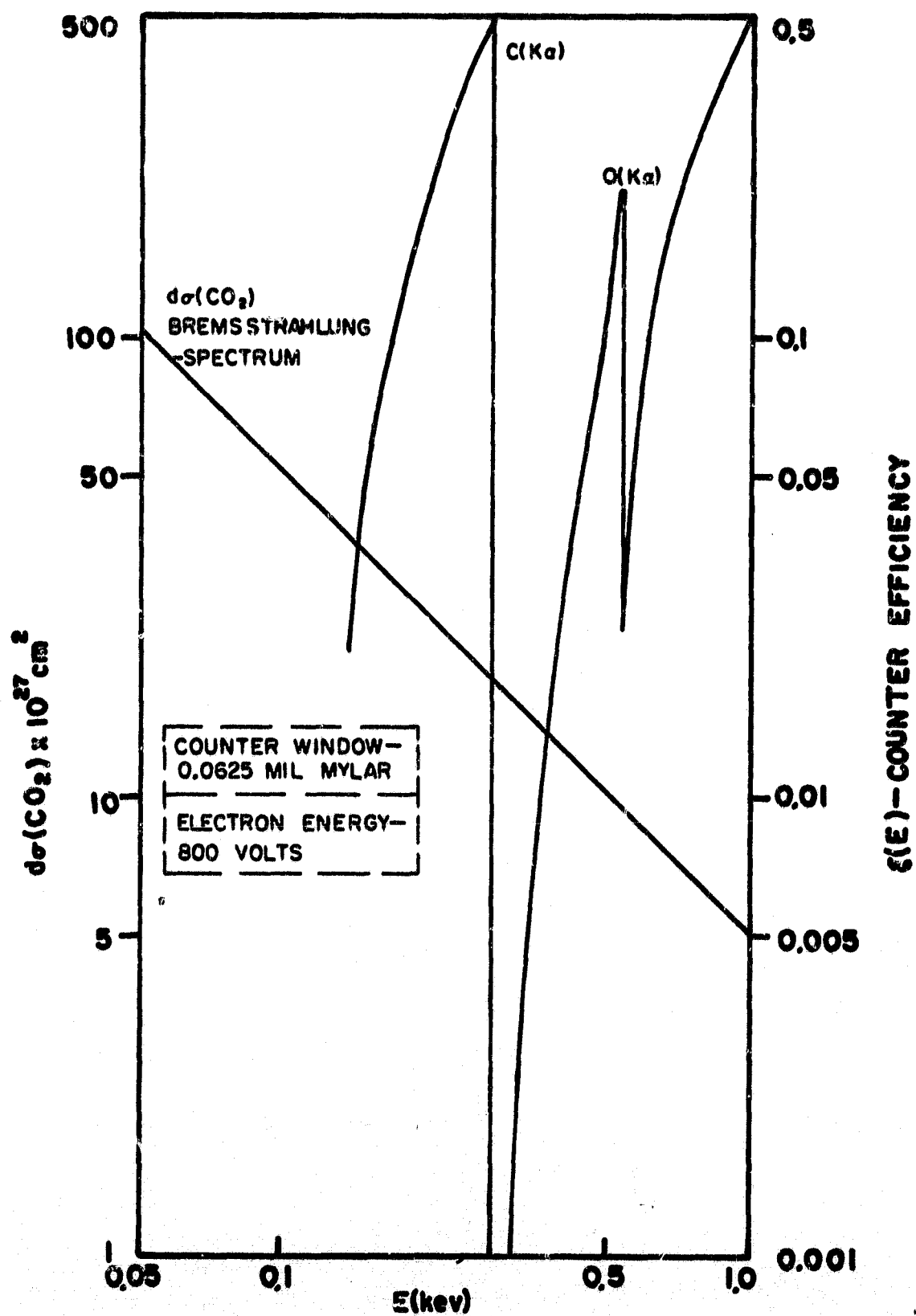
The signal to noise ratio is quite small (~7%) and does not vary significantly with window thickness.

## 6.2 Oxygen K Radiation (23.6 $\overset{\circ}{\text{A}}$ )

We calculated the cross section for k production in oxygen, using 800 volt electrons. Here  $V_k = 525$  volts,  $U = 1.52$  and  $B = 3.05$ . Then  $Q = 0.832 \times 10^{-24} \text{ cm}^2$ . Multiplying by the fluorescence yield (0.0045) we obtain

$$\sigma_k = 3.74 \times 10^{-27} \text{ cm}^2$$

We then calculated the efficiency of a counter having a 0.0025 mil mylar window. Mylar was chosen because of its oxygen edge at 525 ev.  $\epsilon(E)$  is plotted as a function of energy in Figure 6-2. As before,  $d\sigma(E)$  is plotted in the same figure. We evaluated  $\int \epsilon(E) d\sigma$  over the range 0.310 to 0.525 kev. Clearly this underestimates the background. Then  $\int \epsilon(E) d\sigma = 1.5 \times 10^{-26}$  and with  $\epsilon(525 \text{ ev}) = 0.21$  we



COUNTER EFFICIENCY VS ENERGY  
(MYLAR WINDOW)

FIG. 6-2

100870

obtain

$$S/N \leq \frac{\epsilon(E) \cdot \sigma k}{\int \epsilon(E) d\sigma_B} = 0.1$$

10% is too small to be promising considering that we underestimated the background by considering neither the region below 310 ev nor above 525 ev.

## 7.0 CONCLUSIONS

We now summarize the results of our investigations, and indicate a direction for possible future development.

### 7.1 Composition Sensitivity of Bremsstrahlung Gauge

In Section 3.0 we showed that  $Y_A$ , the average X-ray count rate per atom per  $\text{cm}^2$  per incident electron is, to first order, proportional to  $\bar{Z}^2$ , where  $\bar{Z}$  is the average atomic number of a gas atom having an atomic weight of  $\bar{A}$ . Then, if  $n_a$  is the number of gas atoms per  $\text{cm}^3$ , the total flux is given by  $Y_T = C\bar{Z}^2 n_a$ .

C contains only information regarding electron beam current, voltage, and path length along with detector efficiency and solid angle.

But

$$n_a = \frac{N_0}{\bar{A}} \cdot \rho$$

where  $N_0$  is Avogadro's number and  $\rho$  is the mass density in  $\text{gm}/\text{cm}^3$ . Therefore

$$Y_T = C \frac{\bar{Z}^2}{\bar{A}} \cdot N_0 \cdot \rho$$

Thus, for hydrogen, where  $\frac{\bar{Z}}{\bar{A}} = 1$ ,  $\bar{Z} = 1$

$$Y_T \propto \rho \text{ (hydrogen)}$$

and for all other light nuclei, where  $\frac{\bar{Z}}{\bar{A}} \approx \frac{1}{2}$

$$Y_T \propto \frac{1}{2} \bar{Z} \rho$$

Now, from elementary kinetic theory

$$P = K/m \rho T, \text{ where}$$

$K$  = Boltzmann's constant

$\rho$  = mass density

$P$  = pressure

$T$  = absolute temperature

and

$m$  = mass per molecule

Then

$$Y_T = \frac{\bar{Z}^2}{\bar{A}} N_0 \frac{m}{KT} P$$

but

$m = \frac{\xi \bar{A}}{N_0}$  where  $\xi$  is the average number of atoms per molecule. Therefore

$$Y_T = C \bar{Z}^2 \frac{P}{KT} \xi$$

or

$$Y_T \propto \xi \bar{Z}^2 P.$$

Thus we see that in pressure measurements, the yield depends on the chemical state of the residual gas as expressed in  $\xi$ . Density measurements are independent of the chemical state. We computed the response expected on the basis of this simple theory, for a variety of gases including the residual gas

compositions described by Dushman (Ref. 8). We compare the relative sensitivities for density measurement with those for pressure measurement in Table IV. Predictions based on the Sommerfeld-Berger computer output are listed along with typical ion gauge responses as described by Dushman (Ref. 8). This data leads us to the following conclusions:

1. Where computer runs have been made, there is qualitative agreement between the simple theory and the Sommerfeld-Berger computer outputs.

2. Composition sensitivity variations are considerably less when the bremsstrahlung interaction is used for density rather than pressure measurements. This is primarily due to the  $Z^2$  dependence of the yield. For density measurements, the ion gauge and bremsstrahlung gauge are competitive, at least for light elements. Indeed, for hydrogen densities, the bremsstrahlung technique is an improvement.

## 7.2 Ultimate Pressure Limits

For air, the calculated density response at 10 keV is  $1.54 \times 10^{12}$  cps/mA/gm/cc. Experimentally, we determined a pressure response of 3.94 cps/mA/ $\mu$ Torr using a 0.25" diameter collimator (Figure 5-7). Our calculations were made for a different geometry (Figure 3-1), but the difference is less than a factor of 2. If we assume the gas composition to be essentially that of dry air, this converts to a density

TABLE IV  
GAS COMPOSITION SENSITIVITY\*

	N <sub>2</sub>	Air	Ar	H <sub>2</sub>	Oil <sup>†</sup> (A)	Hg <sup>††</sup> (A)
Z	7	7.31	18	1	4.566	71.526
A	14.008	14.55	39.94	1.008	6.6401	161.816
z	2	2	1	2	13.45	1.25
Simple Bremsstrahlung Theory - Relative Response to Pressure P	1	1.092	3.31	0.02	2.87	65.2
Simple Bremsstrahlung Theory - Relative Response to Density ρ	1	1.048	2.31	0.286	0.896	9.04
Sommerfeld-Berger Theory - Rela- tive Response to Density ρ (B) (T <sub>0</sub> = 5 kev)		1		0.197	0.790	7.96
Ion Gauge Relative Response to Pressure P (Experimentally Determined) (C)	1.0		1.32	0.58	2.5	3.56
Ion Gauge Relative Response to Density ρ (Derived From Pres- sure Response)	1.0	0.965	0.925	8.12	0.784	0.493

† Oil Pump & -78°C Trap (A) Dushman, Loc. Cit. P. 208

†† Hg Pump & -78°C Trap (B) Normalized to Air

(C) Dushman, Loc. Ct. P. 324

\*Sensitivity is defined as  $R(x)/R(N_2)$  where  $R(N_2)$  is the gauge response to nitrogen in

$\frac{\text{amp}}{\text{Torr}}$  (ion gauge) and  $\frac{\text{counts}}{\text{amp} \cdot \text{Torr} \cdot \text{sec}}$  (X-ray gauge).  $R(x)$  is the response to gas com-

position X. Using these definitions the sensitivity to N<sub>2</sub> is normalized to 1.

response of  $2.5 \times 10^{12}$  cps/ma/gm/cc. Although the experimental value is a factor of 1.6 higher than the theoretical value, the measured result is not inconsistent with the uncertainties in gas composition, and the differences in the various geometric parameters. In any event we observed reasonable signal to noise ratios at  $5 \times 10^{-5}$  Torr. With appropriate background reduction, we should be able to measure pressures at  $5 \times 10^{-9}$  Torr provided that the detector solid angle is increased. We consider this latter point in Section 7.6.

### 7.3 The Possibility of Using K X-Rays in the Determination of Gas Composition

As we saw in Section 6.0, the possibility of measuring k X-ray intensities in order to determine gas composition is not feasible. The high bremsstrahlung backgrounds and low fluorescence yields of light elements result in extremely low signal to noise ratios.

### 7.4 The Possibility of Determining Hydrogen Concentrations Using the Bremsstrahlung Technique

If we ask whether the bremsstrahlung technique can be used to measure the pressure and density of pure hydrogen, at reduced pressures, the answer is yes. For a given density, response to hydrogen is about 4 times less than the response

to air. At a given pressure, the response is 50 times less for hydrogen. This of course raises the ultimate pressure and density limits.

If instead, the question is whether hydrogen concentrations can be determined in the presence of other gases, the answer is unfortunately no. In fact, we can determine pressure and density only if assumptions are made regarding the average atomic number of the constituent gases.

### 7.5 Advantages of the Bremsstrahlung Gauge

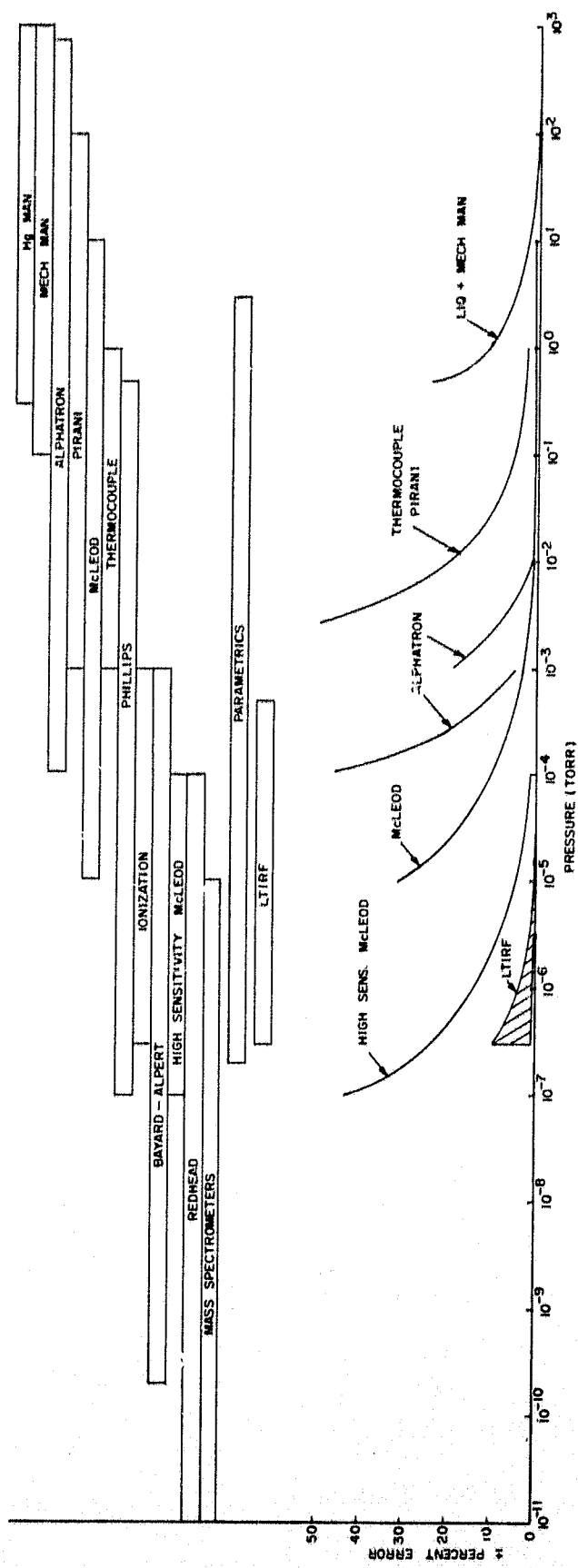
Advantages of the bremsstrahlung gauge are listed below:

- (1) This gauge does not pump the sensitive volume.
- (2) Sensing remote from the electron gun and detector permits sampling volumes located far from system walls.
- (3) Gauge response computations, starting from physical measurements and atomic constants, could qualify this gauge as a primary standard.
- (4) As a secondary or transfer standard, this gauge provides a means of comparing McLeod gauges and ionization gauges. Using a favorable geometry, we could make a measurement with an accuracy of 1% (1 $\sigma$  statistical error) in 16 minutes for a pressure of  $3 \times 10^{-7}$  Torr. Once compared with a McLeod gauge, the bremsstrahlung gauge will maintain its

calibration for a particular gas, so long as the physical configuration and the operating conditions remain unchanged. Operating pressure ranges, shown in Figure 7-1, overlap those available from many other gauges. Gauges labelled "Parametrics" and "LTIRF" refer to bremsstrahlung gauges.

Assumptions used for the Parametrics curve were not specified in the report from which we took this figure. They must include differential pumping of the electron gun to reach pressures above 1000  $\mu$ Torr. Curves labelled LTIRF assume: current of 1 mA; electron gun at ambient pressure; detection of 1/2 the available photons; measuring times of one to ten minutes. Estimates for the LTIRF gauge were added to a figure from an unpublished Technical Memorandum by C. A. Zeigler (1964).

- (5) After suitable development, a bremsstrahlung gauge would need no more space for electronics than a normal ionization gauge. About five inches of rack space provides ample room for power supplies, stabilizers, and counting electronics.
- (6) Gas temperature and degree of ionization do not affect the response of the gauge.



OPERATING RANGES AND ERRORS OF VACUUM GAUGES  
FIG. 7-1

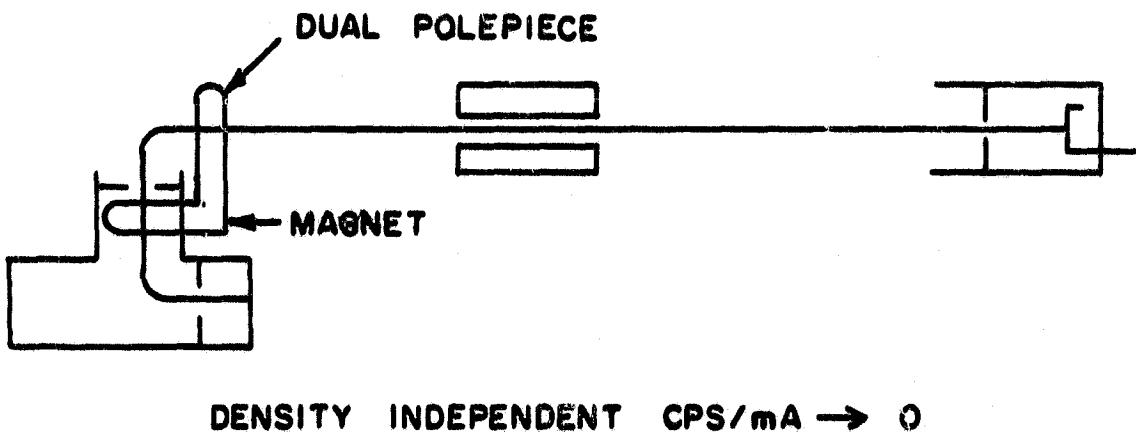
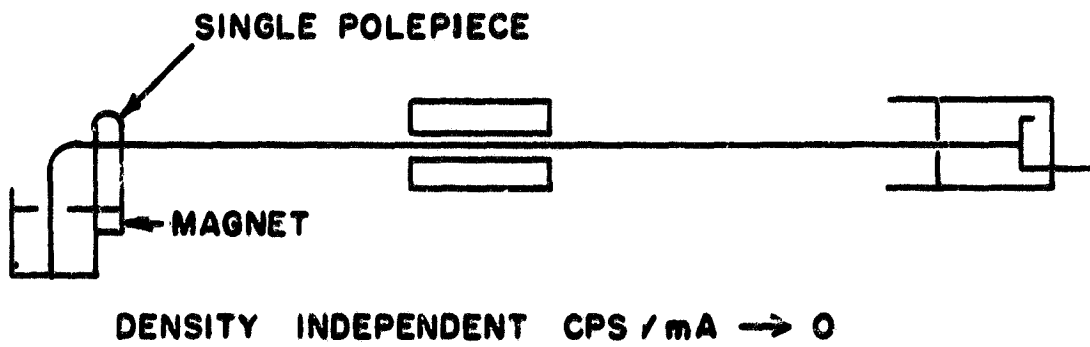
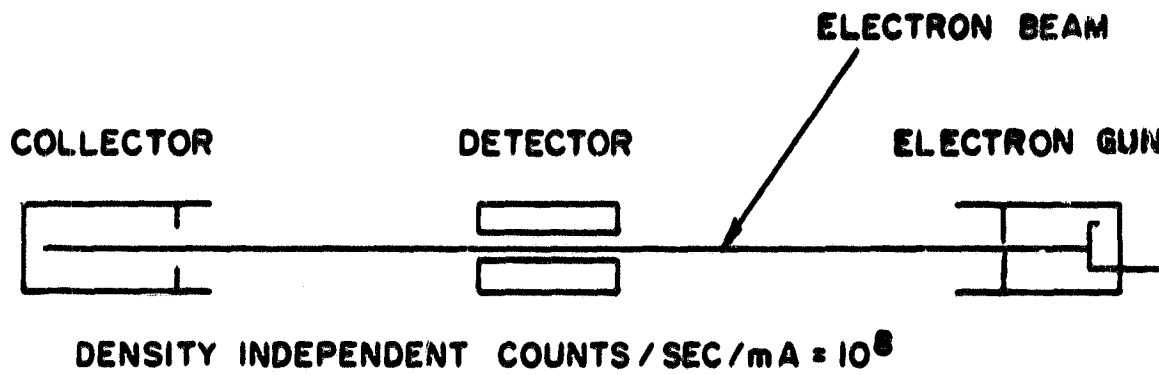
## 7.6 A Technique for Increasing Gauge Sensitivity

X-ray techniques suffer from inverse-square losses arising from separation of source and detector. This geometric efficiency becomes the determining factor in accuracy at low count rates, corresponding in our case to low pressures. No matter how much we improve the response per unit density by other techniques, some fraction of the X-rays escape. In most experiments, the detected energy constitutes only one-thousandth of the available flux.

This arises from a simple computation using common assumptions; the detector lies 10 radii from a point source and the geometric efficiency equals the detector area divided by the surface area of a sphere of radius equal to 10 detector radii, centered at the source. Under these conditions the fraction of X-rays detected cannot exceed .0025 of the total!

We would extend the low-pressure limit by two orders of magnitude if we arranged the detector to capture one-quarter of the emitted radiation.

Assume an experimental arrangement as shown in Figure 7-2. Electrons passing through the center of the cylindrical detector interact with ambient gas molecules and generate bremsstrahlung. Considering the midpoint of the detector axis, only those X-rays that escape through the end openings go undetected. These constitute only about 0.5% of the total. At either end, nearly half the radiation strikes



COLLECTOR SCHEMES TO REDUCE BACKGROUND

FIG. 7-2

the detector. Considerable energy enters from outside the ends of the counter, and only a tiny fraction escapes through the opposite ends. Contributions to the total response from regions located outside the counter at distances greater than five times the entrance diameter can be neglected safely.

Using this detector system, we can detect more than half the radiation generated along the counter length.

We can raise several questions regarding new error sources introduced by the improved geometry.

(1) Electrons scattered from the beam create X-rays when they strike parts of the detector. Bremsstrahlung and characteristic X-rays from the surfaces struck by the electrons create a pressure dependent response. In a carbon-coated system, using a beryllium window, we can expect bremsstrahlung characteristic of materials having  $Z = 4$  and  $6$ . The carbon  $k$  X-ray will not penetrate a beryllium window, but of course the beryllium X-ray will. No response will result from either characteristic X-ray because the energies lie far below  $1$  kev, the level at which we would set the electronic discriminator.

Thick target bremsstrahlung from carbon approximates  $1 \times 10^{11}$  photons/second/mA, into  $4\pi$  steradians while beryllium produces  $2/3$  that number. If even  $1\%$  of the beam electrons struck the detector we would obtain  $10^9$  photons/second, proportional to density via the electron scatter cross section.

(2) Thick target bremsstrahlung from the collector enters the detector at one end and constitutes a pressure independent background.

Even though the detector views the collector directly, no significant background contribution results if the geometric efficiency reduces the flux to low values. Since a tenfold increase in separation produces a hundredfold decrease in flux, relatively small distances may suffice.

Assume a 0.5" detector aperture; then the radius is 0.250", so a collector 2.5 inches away results in a geometric efficiency,  $G$ , of  $2.5 \times 10^{-3}$ . Increasing the separation to  $2.5\sqrt{10}$ " gives  $G = 2.5 \times 10^{-4}$ , while a 25" separation implies  $G = 2.5 \times 10^{-5}$ . Using a factor of 10 increase over the result given by Kramer's Rule we assume  $4 \times 10^{12}$  photons/sec/mA, which could be reduced to  $10^8$  detected photons/sec/mA.

At 5 keV, for air, we expect  $1.8 \times 10^{12}$  photons/second/mA/gm/cc with  $G = 8 \times 10^{-4}$ , thus we could expect  $1.13 \times 10^{15}$  photons/sec/mA/gm/cc with improved geometry. Since air density at normal temperatures equals  $1.56 \mu\text{gm/cc/Torr}$ , we would expect  $1.76 \times 10^9$  photons/second/mA/Torr. Clearly we cannot permit direct viewing of the collector by the detector. The ratio of thick-target X-rays to gas-target X-rays outweighs any practical reduction in geometric efficiency.

These preceding comments apply only when the X-rays originate in the direct view of the detector. Deflecting the electron beam with a local magnetic field at the collector eliminates this problem.

Using a collector like that shown in Figure 7-2, we can bend the electron beam onto a target hidden from the detector. Now only Thompson scattering from the gas can deflect the X-rays into the counter. Using a low-Z target with poor geometric efficiency for X-ray output, and locating the collector far from the detector, one could reasonably provide geometric attenuations of  $10^8$  for photons produced at the Faraday cup. Thompson scatter from the gas contributes a pressure dependent background. From the ratio of cross-sections, this factor approximates  $10^{-4}$ . As a result, using a deflecting collector could reduce the pressure-independent background to zero, and permit only one or two counts/second/mA/gm/cc from Thompson scatter. Correspondingly, unit signal/noise ratio occurs at about  $10^{-11}$  Torr due to cosmic ray background.

Additional Thompson scatter reduction results from bending the electron beam a second time after it enters the collector, thus making the X-rays in a region not directly visible to the entrance aperture. This forces another Thompson scattering event into the chain, giving a further background reduction of  $10^{-4}$ .

## BIBLIOGRAPHY

- 1.) C. A. Ziegler, L. L. Bird, K. H. Olson, J. A. Hull and J. A. Morreal, *Rev. Sci. Inst.*, 35, 450 (1964).
- 2.) A. Sommerfeld, Wellenmechanik (Frederick Unger Publishing Co., New York, 1947).
- 3.) J. M. Berger, *Phys. Rev.*, 105, 35 (1957).
- 4.) J. M. Berger, Table of Non-Relativistic Bremsstrahlung Intensity, Private Communication.
- 5.) R. D. Evans, The Atomic Nucleus, (McGraw-Hill Book Co., Inc., 1955).
- 6.) P. Kirkpatrick and F. Wiedman, *Phys. Rev.* 67, 321 (1945).
- 7.) R and D. Design Evaluation, Density Measurement Rocket Payloads Using Bremsstrahlung, May 1968, AFCRL Report, Contract No. F19628-67-C-0278.
- 8.) S. Dushman, Scientific Foundations of Vacuum Technique (John Wiley & Sons, Inc., 1962).
- 9.) P. Duncumb and S. J. B. Reed, Quantitative Electron Probe Microanalysis, pg. 139, National Bureau of Standards Special Publication 298, 1968.
- 10.) B. Sellers and C. Ziegler, AFCRL Report No. AFCRL-65-307, A Rocket Borne Air Density Measurement System Utilizing Electron-Bremsstrahlung - Design and Development AD-602 682; from this report, the background may be estimated to be .025 cps/ $\mu$ A in a 60 foot diameter sphere.
- 11.) H. A. Bethe, *Ann. Phys., Lpz*, 5, 325 (1940).
- 12.) C. R. Worthington and S. G. Tomlin, *Proc. Phys. Soc. A. (London)* 69A, 401, 1956.
- 13.) E. H. S. Burhop, The Auger Effect, Cambridge University Press, 1952.
- 14.) B. L. Henke, R. L. Elgin, R. E. Lent, and R. B. Ledingham, *Norelco Reporter* 14, 112, (1967).